

GX 17+2: X-ray spectral and timing behaviour of a bursting Z source

E. Kuulkers,¹ M. van der Klis,¹ T. Oosterbroek,¹ J. van Paradijs^{1,2} and W. H. G. Lewin³

¹*Astronomical Institute “Anton Pannekoek”, University of Amsterdam and Center for High Energy Astrophysics, Kruislaan 403, 1098 SJ Amsterdam, The Netherlands*

²*Physics Department, University of Alabama, Huntsville, AL 35899, U.S.A.*

³*Massachusetts Institute of Technology, 37-627, Cambridge, MA 02139, U.S.A.*

Accepted. Received

ABSTRACT

We investigated the properties of the Z pattern of the low-mass X-ray binary GX 17+2 in the X-ray colour-colour diagrams (CDs) and hardness-intensity diagrams (HIDs), and of the power spectra as a function of position in the Z. We used all *EXOSAT* ME data on GX 17+2, a total of 6 observations during 1983–1986. We find that the Z pattern in the CD does not move to within ~ 2 per cent between observations separated by ~ 1 day to ~ 1.5 years. The power spectra and the characteristics of the Z pattern both support the division of the Z sources into two sub-groups, GX 17+2 being in the group together with Sco X-1 and GX 349+2.

It has been noted previously that the maximum frequency of the horizontal branch quasi-periodic oscillations in GX 17+2 is lower than for Cyg X-2, GX 5–1 and GX 340+0. We suggest that an asymmetry in the magnetic field giving rise to polar caps with different emission characteristics may be the origin of this. This may also explain the occurrence of bursts in GX 17+2.

We also report the detection of two new bursts in the *EXOSAT* data of GX 17+2, which we interpret as type I bursts. No regular pulsations are observed during these two bursts nor during the bursts previously detected in GX 17+2 with *EXOSAT*, with upper limits to the pulsed amplitude of ~ 1.5 per cent for pulsations with a frequency below 512 Hz. Three of the four bursts occurred in the normal branch, while one occurred in the lower part of the flaring branch.

The Poisson level in power spectra of data processed by the on-board computer of *EXOSAT* is found to deviate from that expected from simple variable dead time effects in GX 17+2 and also in several other sources. We present corrections to the usually employed relations between count rates observed with *EXOSAT* and the Poisson level.

Key words: accretion, accretion disks – binaries: close – stars: individual: GX 17+2 – stars: neutron – X-rays: bursts – X-rays: stars

1 INTRODUCTION

Studies of the broad-band X-ray spectral and correlated timing behaviour of the brightest persistent low-mass X-ray binaries (LMXBs) have shown that GX 17+2 is one of the six known Z sources (Hasinger & van der Klis 1989), which share many characteristics. In the X-ray colour-colour diagram

(CD) and hardness-intensity diagram (HID) the sources trace out a roughly “Z” shaped track. The limbs of the Z are called horizontal branch (HB), normal branch (NB) and flaring branch (FB), from the top limb to the bottom limb, respectively. The sources move smoothly through the different branches, and do not jump from branch to branch. This one-dimensional motion through the Z is thought to be governed by the mass-accretion rate, \dot{M} , which increases from the HB, through the NB, to the FB (e.g. Hasinger et al. 1990). The Z sources are believed to accrete mass at a rate near the Eddington limit (e.g. Lamb 1989).

* Present address: Astrophysics, University of Oxford, Nuclear and Astrophysics Laboratory, Keble Road, Oxford OX1 3RH, United Kingdom

In each branch, a Z source shows a characteristic power spectrum (Hasinger & van der Klis 1989). In the HB one sees intensity correlated high-frequency (15–55 Hz) quasi-periodic oscillations (QPO), called horizontal-branch oscillations (HBO), together with associated band-limited noise, called low-frequency noise (LFN), which dominates the region from ~ 1 Hz to the HBO frequency. In the NB one sees another type of QPO at a lower frequency (4–7 Hz), called normal-branch oscillations (NBO). NBO have been seen to occur simultaneously with HBO (e.g. Hasinger et al. 1990, Lewin et al. 1992). In some Z sources (Sco X-1, see e.g. Dieters & van der Klis [1996], and GX 17+2, see e.g. Penninx et al. [1990]), the NBO merge smoothly into higher frequency (up to ~ 20 Hz) QPO, called flaring branch oscillations (FBO) when the source moves onto the FB. Recently, kHz QPO have been discovered in the Z source Sco X-1 (van der Klis et al. 1996), whose properties also seem to depend on position in the Z.

Two noise components have been seen to occur in all three branches. One is the very-low-frequency noise (VLFN), dominating the region below ~ 1 Hz. VLFN generally increases towards the FB. The other component is the high-frequency noise (HFN), which dominates the region above ~ 20 Hz. HFN generally decreases towards the FB (see Dieters & van der Klis 1996, and references therein).

It has become clear that on the basis of their spectral and timing behaviour the Z sources can be divided into two categories (Hasinger & van der Klis 1989, Penninx et al. 1991, Kuulkers et al. 1994a), the difference between them may be due to a difference in orbital inclination angle (Hasinger & van der Klis 1989, Hasinger, Friedhorsky & Middleditch 1989, Hasinger et al. 1990, Kuulkers et al. 1994a, Kuulkers 1995, Kuulkers & van der Klis 1995, 1996, Kuulkers, van der Klis & Vaughan 1996) or magnetic field strength of the neutron star (Psaltis, Lamb & Miller 1995)[†]. The Z sources Cyg X-2, GX 5-1 and GX 340+0 form one group, which we shall call the Cyg-like sources, while Sco X-1, GX 17+2 and GX 349+2 form another group, which we shall call the Sco-like sources. The Cyg-like sources have been proposed to have either a higher inclination, or a higher magnetic field, than the Sco-like sources.

The only direct evidence that the compact stars in Z sources are neutron stars is the observation of X-ray bursts from GX 17+2 (Tawara et al. 1984, Kahn & Grindlay 1984, Sztajno et al. 1986) and Cyg X-2 (Kahn & Grindlay 1984, Kuulkers, van der Klis & Van Paradijs 1995, Wijnands et al. 1997, Smale et al. 1996). The irregular occurrence of these X-ray bursts, and the lack of bursts in other Z sources has been attributed to the high mass accretion rate \dot{M} in these systems (see the review by Lewin, Van Paradijs & Taam 1993).

Recently, the *EXOSAT* data of three Z sources have been analyzed in a detailed and homogeneous way (GX 5-1: Kuulkers et al. 1994a, GX 340+0: Kuulkers & van der Klis 1996, Sco X-1: Dieters & van der Klis 1996). The present work reports the results of a similar comprehensive study of the broad-band X-ray spectral and timing behaviour of

GX 17+2. Parts of the *EXOSAT* data on this source have already been reported by Langmeier et al. (1986), Langmeier, Hasinger & Trümper (1990), Sztajno et al. (1986), Stella, Parmar & White (1987), Schulz, Hasinger & Trümper (1989) and Hasinger & van der Klis (1989). In our study we discuss the overall broad-band spectral and timing behaviour within the framework of the magnetospheric model for Z sources and of the idea that GX 17+2 is a Z source with a relatively low inclination. We also report previously unseen bursts, and place all *EXOSAT* bursts within the Z-diagram (a preliminary report of these bursts was given by Kuulkers et al. 1994b).

2 OBSERVATIONS

We analysed all available *EXOSAT* medium energy experiment (ME) argon data (Turner, Smith & Zimmerman 1981, White & Peacock 1988) of GX 17+2. In Table 1 we present the observation log of GX 17+2. The ME had eight detectors, each of which consisted of two layers, an argon filled chamber in front of a xenon filled chamber[‡]. Data were obtained in different observation modes, with good spectral and low time resolution (HER2, HER3, HER4, HER5; the different HER modes gave different options to transmit data from individual detectors or combined from more detectors), or with high time and no spectral resolution (HTR3, HTR4, HTR5). Alternatively, one could obtain data in two (e.g. 1985 day 258/259) or four energy bands (e.g. 1986 day 093/094) at a high time resolution (HER7). A HER mode could be run simultaneously with one of the HTR modes. Either one half of the array of eight detectors (“half 1” [H1] or “half 2” [H2]) was pointed at the source while the other half monitored the background, or the whole array (WA) was pointed at the source (see Table 1).

The HER modes were processed by the *EXOSAT* on-board computer (OBC), which produced large dead-time effects. In our analysis of CDs and HIDs (see below) we determine the dead-time factor from the qualified event rates (collected each 32s for each detector), which are (almost) unaffected by dead time. Of the HTR modes, only the HTR4 mode is processed by the OBC. The HTR4 mode provides the count rate in only one (chosen) energy band at the highest time resolution available with *EXOSAT* (~ 0.25 ms). The HTR4 mode observations on 1985 day 258/259 and on 1986 day 093/094 provided the count rate in the 1.4–11.4 keV band and in the 1.2–19.9 keV band, respectively.

On 1986 February 13th (Thursday, day 044) problems due to atmospheric drag caused by orbital decay started with the *EXOSAT* attitude and orbit control system (AOCS), see White (1986). Between March 27th (day 086) and April 9th (day 099) stable pointing was regained within 5 arcmin. This resulted in a varying collimator response. In principle one could use the star tracker attitude control data (collected every 8 or 16 s) to correct for this. However, due to problems during the 1986 day 093/094 observations with the star trackers and gyros this was not possible for this observation period. We therefore used these data only to produce

[†] If it is due to orbital inclination the Z sources would be intrinsically the same, but appear differently; if it is due to magnetic field, then they would be intrinsically different.

[‡] Early on 1985 day 232 one of the eight detectors ceased to operate.

a CD and not for the HIDs. After April 9th (day 099) stable pointing was lost again, which resulted in a complete loss of the satellite. On May 9th (day 129) *EXOSAT* re-entered the Earth's atmosphere (White 1986).

3 ANALYSIS

For the spectral analysis we use CDs and HIDs. These diagrams are created using either three or four energy bands (e.g. Hasinger & van der Klis 1989). The observations during 1986 day 093/094 provided four energy bands, so we decided to analyse all the data using energy boundaries corresponding to these bands. We found that three energy bands (i.e. combining two of the four bands) gave the best separation of the branches of GX 17+2 in the CD: 1.2–4.7 keV, 4.7–6.6 keV and 6.6–19.9 keV. In the CD and HIDs the soft colour is defined as the ratio of the count rate in the second energy band to the count rate in the first energy band, while the hard colour is defined as the ratio of the count rate in the third energy band to that in the second energy band. The ‘intensity’ used in the HIDs is the count rate per cm^2 in the 1.2–19.9 keV band, corrected for dead time and collimator response (as redetermined by Kuulkers et al. 1994a). The count rates were corrected for background. All points in the CD and HIDs are 200 s averages.

In order to investigate the fast timing behaviour of GX 17+2 we performed fast Fourier transforms (FFTs) on successive 16 s and 512 s blocks of data of all the high-time resolution argon data. Power spectra of blocks of 512 s of data were used to study primarily the low-frequency behaviour <1 Hz. In order to obtain a more accurate binning in position in the Z, we used the power spectra of 16 s blocks of data. The latter power spectra were used to study primarily the high frequency (>1 Hz) behaviour. The power spectra were grouped according to position in the Z and then averaged.

When analysing power spectra of Z sources, one encounters several power spectral components (Hasinger & van der Klis 1989): a constant level due to counting noise (the so-called Poisson level) modified by dead-time processes, three “noise” components, VLFN, LFN and HFN, and two kinds of QPO, HBO and NBO/FBO. In some cases the HBO show a second harmonic, which is also represented by a Lorentzian. For completeness we give the functional shapes of these components (see also Hasinger & van der Klis 1989, Kuulkers et al. 1994a):

The VLFN is given as: $P_{\text{VLFN}}(\nu) = A_V \nu^{-\alpha_V}$, where ν is the frequency, α_V the power-law index, and A_V the normalization constant.

The LFN and HFN are given as: $P_{\text{Noise}}(\nu) = A_N \nu^{-\alpha_N} e^{-\nu/\nu_N}$, where α_N is the power-law index, ν_N the cut-off frequency, and A_N the normalization constant. In the Z sources α_N was usually found to be consistent with zero for the HFN component (Hasinger & van der Klis 1989, see also Dieters & van der Klis 1996), and we fixed the parameter at this value. In Tables 2, 3a and 3b we use the subscript L and H for the LFN and HFN components, respectively.

The HBO, their harmonic, the NBO and the FBO are broad peaks with centroid frequencies ν_c . These peaks are described by Lorentzians: $P_{\text{QPO}}(\nu) = A_Q[(\nu - \nu_Q)^2 +$

$(\Delta\nu_Q/2)^2]^{-1}$, where $\Delta\nu_Q$ is the full width at half maximum (FWHM) of the QPO and A_Q a normalization constant.

The strengths of the various noise components are expressed in terms of the fractional rms amplitudes of the corresponding fluctuations in the time series. They are calculated by integrating their contributions to the power spectra over certain frequency ranges, as determined from fits of the functional shapes given above to the power spectra. The VLFN was integrated in the 512 s power spectra over the range 0.001 to 1 Hz, and in the 16 s power spectra over the range 0.01 to 1 Hz. For the LFN and HFN we integrated over the range 0.01 to 100 Hz. Note that in the 16 s power spectra we extrapolated the power spectral shapes from ~ 0.06 Hz down to 0.01 Hz. The HER7 and HTR4 data suffer from large variable dead time effects. We corrected the fractional rms amplitudes of the power spectral components for these effects (see van der Klis 1989, Kuulkers et al. 1994a).

The Poisson levels of the power spectra from non-OBC processed data, the HTR3 and HTR5 modes, were determined using the known relation between Poisson level and observed raw count rate for these modes (Van der Klis 1989, Berger & van der Klis 1994). In power spectra from OBC-processed data, the HER7 and HTR4 modes, the OBC dead time strongly affects the Poisson level (see e.g. Kuulkers et al. 1994a). Moreover, the power spectrum of the Poisson noise in these power spectral data can no longer be considered constant at frequencies higher than ~ 120 Hz; it increases to higher frequencies (Tennant 1987). Most HER7 mode data had a Nyquist frequency of 128 Hz or lower, so this only had a significant effect in the HTR4 mode, which had a Nyquist frequency of 2048 Hz. We used the Poisson level as a free parameter in the fits to the HER7 power spectral data. In the case of HTR4 we first binned the data to a time resolution of ~ 4 ms, and used the Poisson level as a free parameter in the power spectral fits. We refer to Appendix A for a more detailed discussion of dead time effects.

Whenever a power spectral component was not clearly present in the averaged power spectra, we determined a 1σ upper limit to the rms amplitudes of this component by fixing its other parameters (while keeping the parameters of the other observed components free). The values of the fixed parameters were determined by evaluating the observed behaviour (using only the HTR-mode data) of the corresponding components when they were clearly detected, and are discussed below.

VLFN is present in all branches. Since there is no simple dependence of the VLFN power-law index as a function of the position in the Z (Section 4.2.2) we fixed it to its average observed value when determining an upper limit, i.e. 1.5.

LFN is observed to be only present in the HB and the upper part of the NB. Upper limits where therefore only determined for S_Z (see Section 4.2.1) up to ~ 1.35 . No clear dependence of the LFN power-law index and cut-off frequency on position in the Z is found (Section 4.2.3); the fixed values when upper limits were determined of these parameters were, therefore, -0.5 and 2 Hz, respectively.

HFN is also present in the whole Z, but no clear dependence of the HFN cut-off frequency as a function of the position in the Z can be found (Section 4.2.4). In cases when an upper limit was determined the cut-off frequency was fixed at ~ 77 .

The HBO centroid frequency clearly depends on position in the HB (Section 4.2.5, see also Penninx et al. 1990). The power spectral fit results from HTR3-mode data on 1985 day 258/259 (Table 3a) indicate the following linear relation between the centroid frequency and S_Z : $\nu_{\text{HBO}} (\text{Hz}) = 24.0 + 12.5 S_Z$. This relation was used when an upper limit on the HBO was determined; for the HBO FWHM no clear dependence on the position in the Z is found (Section 4.2.5) and we then fixed it at 3.

A clear HBO harmonic was only detected on a few occasions (see Table 4, later). Whenever the fundamental HBO was clearly detected we determined an upper limit on its harmonic. In these cases the harmonic centroid frequency and harmonic FWHM were fixed to twice the value of the fundamental frequency and fundamental FWHM, respectively, whenever the source was in the HB. Recently, QPO between 50 and 62 Hz were found in the upper and middle part of the NB of GX 17+2 (Wijnands et al. 1996a). We regard this as the HBO harmonic (see Section 6.2.2). Between S_Z values of 1–1.75 we determined rms amplitude upper limits for such QPO using fixed values for the centroid frequency of 60 Hz and FWHM of 5 Hz.

Upper limits to the NBO rms amplitude were determined in the entire NB. Average values of 3 Hz and 7 Hz were then used for the fixed centroid frequency and FWHM, respectively.

Upper limits to the FBO rms amplitude were determined in the entire FB. We then fixed its centroid frequency and FWHM to the observed value, i.e. 16 Hz and 7 Hz, respectively.

4 SPECTRAL AND TIMING BEHAVIOUR

4.1 Broad-band spectral analysis

The CD of all HER observations after 1983 is shown in Fig. 1a. In Figs. 1b and c we display the corresponding HIDs, with the 1986 data, which had pointing problems, left out. The CD and HIDs of the 1983 day 215/216 data can be found in Figs. 2a–c. The data points in these figures have been connected to show more clearly the presence of the FB. It appears that the 1983 Z track is at higher soft and hard colours than that of the other observations. The overall intensities are comparable. CDs of other sources show similar shifts between data for a certain period in 1983 and later data. This was observed in the Z sources GX 5–1, Cyg X-2, GX 349+2, and the atoll sources 4U 1636–53 and Ser X-1 (see Kuulkers et al. 1996, and references therein). Since all sources show the same effect, the shift is probably instrumental.

All data on GX 17+2 obtained after 1983 fall within a single Z track in the CD. We can exclude shifts in the soft and hard colours at the level of $\sim 2\%$ (determined by examining the width of the branches). We therefore conclude that the Z track of GX 17+2 in the CD is stable to within ~ 2 per cent and does not show evidence for secular motion in the CD for observations separated by ~ 1 day up to ~ 1.5 years.

The HIDs of GX 17+2 seem to be also quite stable. However, one data set (1985 day 259) is placed at ~ 8 per cent higher intensities than the other data. Since instrumental changes between the 1984 day 249/250 and the 1985 day

258/259 data can only be expected to contribute at most up to 3 per cent in intensity (see Kuulkers & van der Klis 1996) we think this shift in intensity is probably intrinsic to the source. More observations are needed to verify if this effect is real and how it relates to other source properties.

As can be seen in Figs. 1a–c and 2a–c, GX 17+2 was observed in all three spectral branches (see also Table 1). The HB is clearly not horizontal in the CD, but nearly vertical, as noted previously (e.g. Hasinger & van der Klis 1989); in the other diagrams it has different orientations. Due to an unfortunate choice of HER7 energy boundaries when the 1986 observations were performed, the FB is positioned close to the NB (Fig. 4a). This also caused the FB to be oriented above the NB in Fig. 2b, while it falls along the NB in Fig. 2c.

4.2 Power spectral analysis

4.2.1 Introduction

We studied the power spectral components as a function of position along the Z. We used a one-dimensional parameter, S_Z to measure curve length along the Z (Hertz et al. 1992, Dieters & van der Klis 1996). The scale in the CD was fixed by assigning S_Z values of 1 and 2 for the HB/NB apex and the NB/FB apex, respectively, in the CD of Fig. 1a. The same scaling was also used for the 1983 day 215/216 observations. We note that during the first part of the 1985 day 258/259 observation (16:15–03:13 UT) we could not estimate S_Z from the CD, since data were only available in one broad low energy band. However, since the position in the HB is dependent on intensity we could determine S_Z indirectly. For the second part of the 1985 day 258/259 observation we had sufficient data to determine the dependence of intensity on S_Z in the relevant channel. We used this relation to determine S_Z values in the first part of the observations. Using the above defined scaling we find that S_Z ranges from ~ 0 in the upper part of the HB, to ~ 4.5 in the upper part of the FB. In Figs. 3a–c we show average power spectra from the different branches (HB, NB and FB). The various spectral components are indicated.

In Tables 2, 3a and 3b we give the results of the power spectral fits as a function of S_Z for the 512 s and 16 s data segments, respectively. In Table 4 we give the results for the HBO harmonic (see Section 4.2.5). Upper limits (1σ) have been determined on the rms amplitudes whenever a component was not clearly present in the average power spectra. The range in S_Z where these upper limits were determined and the values to which the other parameters of that particular component were fixed are described in Section 3.

In Figs. 4a–l most of the power spectral parameters have been plotted vs. S_Z . In the next sections we discuss the results for each power spectral component. The 1985 day 258/259 HER7 and HTR4 data are not used in our discussion since they have different energy bands than the other data (see Table 1); only for the discussion of the HBO FWHM and frequency we include the HTR4 data, since these parameters are approximately independent of the energy (Penninx et al. 1990, Penninx et al. 1991, Lewin et al. 1992).

4.2.2 Very-low-frequency noise (VLFN)

The VLFN was detected in all spectral branches, consistent with previous observations. The VLFN rms and its power law index are plotted vs. S_Z in Figs. 4a and b, and Figs. 4c and d, for the 512 s FFTs and 16 s FFTs, respectively. We did not include the 1986 day 093/094 data, which had VLFN rms values between 5 and 6 per cent (Table 2), while in the other observations in the lower part of the NB the rms is around 1 per cent. We attribute this to the intensity variations arising from the changing collimator response on time scales longer than ~ 100 s, which causes leakage of power from lower frequencies into the passbands of the power density estimators with nominal frequencies in the VLFN frequency range (see Deeter 1984). The power law index during the 1986 093/094 observations is about 2, consistent with low frequency leakage.

The changing collimator response only affects frequencies below 0.01 Hz. This is clear from Figs. 4c and d, where the 1986 day 093/094 VLFN components, here measured only down to 0.01 Hz, fall along the other data points in both figures.

The VLFN rms is lowest (~ 0.5 per cent) in the upper part of the HB and the upper part of the NB. It shows a local maximum in the middle part of the HB of ~ 1 per cent. From the upper part of the NB to the lower part of the NB the rms increases to ~ 1.5 per cent. From the 16 s FFTs we infer that the VLFN strength continues to rise from the lower part of the FB to the upper part of the FB, up to at least 3 per cent.

In the lower part of the NB the power law index has values of ~ 1.5 . In the upper part of the FB the power law index is about 2, as expected from leakage effects from slow (source) intensity variations (see above).

4.2.3 Low-frequency noise (LFN)

The LFN is peaked (see e.g. Fig. 3a) as is clear from the negative LFN power law index values between -1.5 and 0, with cut-off frequencies between 1 and 3 Hz. In Figs. 4e, f and g we show the LFN rms, power law index and cut-off frequency, respectively, as a function of S_Z . The rms of the LFN decreases from ~ 3 per cent in the upper part of the HB to ~ 1.5 per cent in the upper part of the NB (see also Tables 2 and 3a).

The low rms and the large uncertainty in the LFN cut-off frequency in the upper part of the NB indicate that the LFN vanishes in this part of the NB. In the rest of the NB and in the FB no evidence for LFN was found.

4.2.4 High-frequency noise (HFN)

The HFN is also present in all branches, see Figs. 4h and i for the 512 s FFTs, and Table 3a and 3b for the 16 s FFTs. Like the VLFN, the HFN is not correlated with any of the other power spectral components. The rms strength clearly decreases from the upper part of the HB to the middle part of the NB from ~ 5.3 per cent to ~ 2.5 per cent. From there onwards it remains between 2 and 3 per cent.

The cut-off frequency is not well determined in many of the power spectra, mainly due to the relatively low Nyquist frequencies (64 Hz) in the 1984 day 249/250 and 250/251

data. Whenever it could be determined we found values between 10 and 50 Hz.

4.2.5 QPO: HBO, NBO and FBO

HBO were only found in the 1985 day 258 data in the upper part of the HB (Tables 2, 3a and 3b, Fig. 3a). There are indications of a very weak HBO component in the expected frequency range in the 1984 day 249/250 data, but this component is not significant. The QPO frequency increases from ~ 23 to ~ 28 Hz from the upper part of the HB to the middle part of the HB, while the FWHM and rms decrease from ~ 7 to ~ 2 Hz and ~ 2.5 per cent to ~ 1 per cent, respectively. The HBO disappear below ~ 1 per cent rms in the lower part of the HB.

A harmonic to the HBO peak with a frequency consistent with twice the HBO frequency is seen at the lowest S_Z values (see Table 4, Fig. 3a). The harmonic has a FWHM between 10 and 20 Hz and an rms of about 2.5 per cent. The harmonic is about as strong as the HBO itself; the data do not allow to distinguish between the harmonic peak being the same width, or twice as wide, as the main peak (see also Table 4).

NBO with frequencies between 5 and 7 Hz were only detected in the middle and lower part of the NB (Fig. 3b), with an rms between 1.5 and 2.5 per cent, and FWHM between 2 and 6 Hz (Figs. 4j–l).

In the 1986 day 093/094 data we found evidence for FB QPO (FBO) in the lower part of the FB (Fig. 3c), with a centroid frequency of ~ 16 Hz, FWHM of ~ 7 Hz and rms of ~ 2 per cent.

5 BURST ANALYSIS

5.1 New bursts

In Figs. 5a–e we show the light curves of all observations (except 1986 day 093/094) at 5 s time resolution. In Figs. 5c and d the smooth overall variations are interrupted by two bursts, which were already reported by Sztajno et al. (1986). In Figs. 5a–e we indicated which spectral branch the source was in at each instant.

As noted in the previous section, the pointing during observation 1986 day 093/094 was only stable to within 5 arcmin. In Fig. 6 we display this data set (Fig. 6a, 5 s time resolution) together with a soft-colour curve (Fig. 6b, 200 s time resolution). Although variations due to the varying collimator response are visible, one can also see that the variations in the FB are more irregular than in the NB.

Two sharp peaks seem to disturb the relatively smooth variations in the light curve of the 1986 day 093/094 data ($\sim 36\,000$ and $\sim 104\,000$ s after the start of the observations). We investigated these peaks and found that they are X-ray bursts which had been previously overlooked. The house-keeping data ruled out a solar particle origin (see also e.g. Kuulkers et al. 1995). In Figs. 7a and b we display light curves of these bursts at a higher time resolution (0.5 s); plotted is the total HTR5 count rate, corrected for dead time and background. The second burst straddled two *EXOSAT* observation segments and is therefore interrupted for

~200 s. The housekeeping monitoring during this time interval still provided 32 s resolution qualified event rate data with which we overlayed the HTR5 light curve of this burst.

The bursts are not related to the changes in the pointing of the satellite. The events rise within 1 s, which is much faster than the pointing variations (typically ~100 s), and show clear hardness variations, which can not be caused by pointing variations. In Figs. 7c and d we display the 4.7–19.9 keV/1.2–4.7 keV hardness ratio curves of the two bursts. The bursts display spectral softening during their decay.

5.2 Burst properties

The first of the two new bursts started at 1986 day 093 14:04:57 (UT) and lasted for ~100 s, while the second started ~19 hr later at 1986 day 094 9:05:40 (UT) and lasted ~300 s. No other bursts occurred in between these two during times that the OBC was operational. We checked whether bursts occurred when the OBC was not operational using the housekeeping data, and found none. Since the collimator response changed on time scales of ~100 s during these bursts, it was not possible to accurately determine the standard X-ray burst parameters (see Lewin et al. 1993) α (ratio of the average persistent flux to the time-averaged flux emitted in the bursts) and γ (ratio of the mean persistent pre-burst flux and the net peak burst flux). However, it is clear that α was very large (larger than 1000) and $\gamma > 1$. Spectral data (HER2) were only available during the second burst, but because the burst was interrupted and was observed with an uncertain, varying collimator response, we did not analyze these data.

To investigate in which branch the source was when the 1986 bursts and the bursts detected by Sztajno et al. (1986) occurred, we indicated the position of the soft and hard color values in the CD at the time the bursts occurred with arrows in Fig. 1. We found that the small 1984 day 250 burst (I) occurred when GX 17+2 was in the upper part of the NB, while the other bursts (1985 day 232: II; 1986 day 093: III; 1986 day 094: IV) occurred in the middle part of the NB or near the NB/FB apex. Although none of the bursts occurred in the HB, we note that GX 17+2 is only occasionally found in the HB (see Section 6.1). Moreover, using the total time spent in each branch as observed with EXOSAT, we found that the occurrences of the four EXOSAT burst are consistent with being independent of branch position. We also found no clear relation between burst duration and position in the Z.

5.3 Pulsations during the bursts?

We searched for periodicities in the bursts. We followed the same procedure for searching pulse periods as Vaughan et al. (1994). We transformed 16 s, 256 s and 64 s data segments for the 1984, 1985 and 1986 bursts, respectively. We also averaged the power spectra of 64 s data segments of the two 1986 bursts, and of these bursts together with the 1985 burst. We found no evidence for a periodic signal above the 99 per cent confidence detection level. The 99 per cent confidence upper limits to the amplitude of a sinusoidal modulation are given in Table 5. The best limits are ~1 per cent for the 0–256 Hz frequency range, and ~1.5 per cent for the 256–512 Hz frequency range.

6 DISCUSSION

6.1 Two groups of Z sources

GX 17+2 and the other Z sources form a group with similar behaviour, i.e. three branches with correlated fast timing behaviour (Hasinger & van der Klis 1989). However, it has been shown that GX 17+2 shares properties with Sco X-1 and GX 349+2, which are distinct from GX 5–1, Cyg X-2 and GX 340+0 (Hasinger & van der Klis 1989, Penninx et al. 1991, Kuulkers et al. 1994a). The latter sources, for example, show long-term variations in the position of the Z pattern in the CD by typically ~7 per cent (which are recurrent in position and shape in the case of Cyg X-2, see Kuulkers et al. 1996) and dipping behaviour in the FB, while the former sources show a more stable Z pattern and flares in intensity in the FB. In this paper, we showed that in the CD the position of the Z track of GX 17+2 is stable to within 2 per cent, which is in accordance with this.

It has been suggested that these differences are caused by a difference in orbital inclination angle (Kuulkers et al. 1996, and references therein). Optical observations of Cyg X-2 (Cowley, Crampton & Hutchings 1979) and Sco X-1 (Crampton et al. 1976) indicate orbital inclinations of 65–75° and 15–40°, respectively. The fact that intensity decreases in the FB of the Cyg-like sources is interpreted as obscuration of the central emission by the inner disk when it swells up as the luminosity approaches the Eddington limit. Orbital inclination also plays a key role in suggested explanations for: (i) the secular variations in the shape and position in the CD and HID of the Z pattern of the Cyg-like sources (e.g. Kuulkers et al. 1994a, 1996), (ii) the shortness of the FB in GX 5–1 (Kuulkers & van der Klis 1995) and (iii) the peculiar QPO found in the FB of Cyg X-2 (Kuulkers & van der Klis 1995). For example, long term variations may be caused by changes in our view of the inner regions due to changes in the geometry of structures near the orbital plane (such as accretion stream and outer disk, see Kuulkers et al. 1994a, 1996, see also Wijnands, Kuulkers & Smale 1996b).

Several other properties (described below) in Z sources also appear to correlate with the division into two groups, but have not (yet) been interpreted in terms of orbital inclination differences.

Peaked LFN has been observed in GX 17+2 and Sco X-1 (see e.g. Hasinger & van der Klis 1989), while all three Cyg-like sources show non-peaked LFN. Atoll sources also show peaked and non-peaked noise (the so-called atoll source HFN). It has been suggested that atoll source HFN is similar to Z source LFN (van der Klis 1994). The different HFN shapes in atoll sources could perhaps be a manifestation of similar effects to those seen in Z source LFN.

A vertical (short) HB in the Sco-like sources has been seen, versus a horizontal HB (with an upward bend at the lowest \dot{M}) in the Cyg-like sources.

The following property also appears different between the two groups, but seems hard to fit in with the orbital inclination framework: GX 17+2 and Sco X-1 are only occasionally found in the HB, and GX 349+2 never, while GX 5–1, Cyg X-2 and GX 340+0 are frequently found in the HB, but only occasionally in the FB. Moreover, the Sco-like sources spend a much longer time scale in the FB (>12 hr) than the Cyg-like sources (<2 hr). Since there is a good evidence that M

increases from the NB to the FB this implies that, on average, the Sco-like sources have a higher \dot{M} than the Cyg-like sources. It is hard to understand how this could have its origin in the inclination at which we view the sources, unless viewing geometry affects the \dot{M} level at which branch transitions occur in the CD and HIDs. Careful study of fast timing properties as a function of S_Z can in fact show whether this is the case, but the available data are not sufficient to make a strong case either way.

Recently, Psaltis et al. (1995) suggested the magnetic field strength of the neutron star to be the origin of the differences in the shape of the Z track in the Cyg-like and Sco-like sources (the magnetic field being lower in the latter sources). From their radiative transfer calculations they infer that subtle differences in the magnetic fields are able to explain the observed differences in the shapes of the Z pattern. It is not clear whether a difference in neutron star magnetic fields can explain the shifts in the Z track position, the apparent difference in mean \dot{M} between the two groups, or the differences in LFN shape, but it does seem likely that differences in HBO properties between the two groups can be explained by it.

6.2 Timing behaviour

6.2.1 Very-low-frequency noise

The VLFN was detected in all branches. Near the HB/NB vertex it was weakest (~ 0.5 per cent rms), while in the FB it was strongest (rms of up to at least ~ 3 per cent rms). We found power law indices between ~ 0.8 and ~ 2 .

The VLFN of Z sources has been investigated in detail in several other studies as a function of S_Z (GX 5-1: Kuulkers et al. 1994a, *EXOSAT* argon; Sco X-1: Dieters & van der Klis 1996, *EXOSAT* xenon; Hertz et al. 1992, *Ginga*; GX 340+0: Kuulkers & van der Klis 1996) or as a function of rank number (GX 5-1: Lewin et al. 1992, *Ginga*; Cyg X-2: Hasinger et al. 1990, Wijnands et al. 1996c, *Ginga*; Hasinger 1993 [private communication], *Ginga* and *EXOSAT* argon; GX 340+0: Van Paradijs et al. 1988a, *EXOSAT* argon; Penninx et al. 1991, *Ginga*; GX 17+2: Penninx et al. 1990, *Ginga*). Hasinger & van der Klis (1989) investigated *EXOSAT* data of the six Z sources as a function of HB, NB and FB. Comparing the *EXOSAT* argon and the *Ginga* results (both instruments provided roughly the same energy range), we find that the VLFN is lowest in the upper part of the NB, near the HB/NB vertex. The minimum strength is similar for all the sources, i.e. near 0.5 per cent rms. The increase in VLFN from the upper part of the NB to the lower part of the FB is strongest in GX 5-1 (Kuulkers et al. 1994a) and Cyg X-2 (Hasinger 1993, private communication). The VLFN rms near the NB/FB vertex is ~ 4 per cent in GX 5-1 (Kuulkers et al. 1994a), while it is about 2 per cent for GX 340+0 (Van Paradijs et al. 1988a, Penninx et al. 1991), GX 17+2 (this paper) and Sco X-1 (Hertz et al. 1992). The sources GX 5-1 and GX 17+2 show evidence for a maximum of ~ 1 per cent in the middle part of the HB (Kuulkers et al. 1994a and this paper, respectively). As shown by Dieters & van der Klis (1996), the VLFN is stronger in the 5–35 keV xenon data (see also Stella et al. 1987), i.e. at higher energies.

The power law indices for GX 340+0 (Penninx et al.

1991), GX 17+2 (Penninx et al. 1990, this paper) and Sco X-1 (Hertz et al. 1992, Dieters & van der Klis 1996) show more or less the same behaviour as a function of S_Z . The index is low ($\lesssim 1$) in the HB and upper part of the NB, while it increases to ~ 2 near the NB/FB vertex. In the FB VLFN power law indices around 2 have been found (note that the true values could be even higher, due to the leakage of power in the VLFN frequency range). GX 349+2 (Hasinger & van der Klis 1989) shows behaviour consistent with this. GX 5-1 (Kuulkers et al. 1994a) shows a clearly opposite behaviour. The power law index remains at about 2 along the HB to the middle part of the NB, and then drops to ~ 1.4 in the lower part of the FB.

In the model of Lamb (1989) the increase of VLFN from the lower part of the NB into the FB is explained by instabilities in the accretion flow. When \dot{M} reaches the Eddington limit radiation pressure becomes important. Accretion onto the neutron star becomes highly unstable at this stage, and therefore increases the VLFN strength.

6.2.2 Horizontal branch QPO

In the upper/middle part of the HB we found HBO with frequencies between 24 and 28 Hz, FWHM between 1 and 8 Hz, and fractional rms amplitudes between 1.5 and 2.5 per cent. The HBO decreased rapidly in strength from the upper part of the HB to the middle part of the NB. We found evidence for a second harmonic, with a frequency consistent with twice the HBO frequency, and with similar strength as the first harmonic. These results are similar to those reported by Stella et al. (1987) and Langmeier et al. (1990) for the *EXOSAT* data. The range of the HBO frequencies falls within the range (18–30 Hz from upper to lower part of the HB) found by Penninx et al. (1990) in *Ginga* data.

More recently, variable-frequency QPO have been found on the NB of GX 17+2 (Wijnands et al. 1996a). These authors interpreted these QPO as being (fundamental) HBO which persists on the NB. However, if we extrapolate the (linear) relation between HBO fundamental centroid frequency and S_Z , using our HTR-mode EXOSAT data, we find a frequency of ~ 36.5 Hz at the HB/NB vertex ($S_Z=1$), which is near the maximum value found in the lower part of the HB in the *Ginga* data (see above). A similar conclusion can be derived from the *Ginga* power spectral parameters for the HBO (Penninx et al. 1990). Extrapolating the (linear) relation between HBO fundamental centroid frequency and either *Ginga* MPC3 colour or *Ginga* PC colour to ~ 60 Hz give HB/NB vertex colour values which are way off from the expected place of the vertex in the *Ginga* CD and HID. We therefore interpret the variable-frequency QPO as being a harmonic of the HBO, unless the HBO fundamental centroid frequency changes abruptly (by 15–20 Hz) near the HB/NB vertex. The linear change of the HBO harmonic centroid frequency (see Penninx et al. 1990) as a function of either *Ginga* MPC3 colour or *Ginga* PC colour, extrapolated to the expected HB/NB vertex in the *Ginga* CD and HID are consistent with this interpretation.

The other Z sources in which HBO have been found, GX 5-1 (Lewin et al. 1992, Kuulkers et al. 1994a), Cyg X-2 (Hasinger 1987a, Hasinger et al. 1990, Wijnands et al. 1997) and GX 340+0 (Penninx et al. 1991, Kuulkers & van der Klis 1996) show HBO properties that are somewhat different

from those of GX 17+2. The maximum HBO frequencies are much higher in the former sources (up to 55 Hz, with rms amplitudes between 2 and 6 per cent). In GX 5–1 a second harmonic with an rms amplitude roughly half that of the first harmonic was found (Lewin et al. 1992, Kuulkers et al. 1994a); similar harmonics are reported in the HBO of Cyg X-2 (Hasinger 1987a, Focke 1996, Wijnands et al. 1997) and GX 340+0 (Kuulkers & van der Klis 1996).

The HBO are thought to be caused by magnetospheric gating (Alpar & Shaham 1985, Lamb et al. 1985, Ghosh & Lamb 1992), at the beat-frequency between the neutron star spin frequency (ν_{NS}) and the Kepler frequency at the inner disk edge (ν_{K0}). This beat-frequency model requires inhomogeneities in the accretion flow, whose presence has as a natural consequence the production of LFN. The radius of the inner edge of the disk depends on \dot{M} , the magnetic moment μ and the mass M of the compact object (Ghosh & Lamb 1992). For n-fold symmetry in the magnetic field pattern, this leads to (see Lamb et al. 1985, Ghosh & Lamb 1992):

$$\nu_{\text{HBO}} = n(C\dot{M}^{\alpha} \mu^{\beta} M^{\kappa} - \nu_{\text{NS}}), \quad (1)$$

where n is the harmonic number, C is a constant, and α , β and κ are exponents which depend on the particular inner disk model considered; $\alpha > 0$, $\beta < 0$, whereas κ can be either positive or negative. There are various ways to produce the \sim factor 2 lower HBO frequency range in GX 17+2 as compared to the other Z sources: lower the overall mass-accretion rate, increase the magnetic field strength or the mass of the neutron star, either increase or decrease the spin period of the neutron star depending on the value of κ , or lower the harmonic number n (if $n > 1$). Of these possibilities, differences in \dot{M} and M are unlikely. \dot{M} is probably the same at the apexes for all Z sources (e.g. Lamb 1989, Hasinger et al. 1990). (But perhaps the inclination influences the position of the apexes in an unknown way, see also Section 5.2.) Unless κ is large, neutron star masses are not likely to be sufficiently different to explain a factor of 2 in the maximum HBO frequency. A closer match between ν_{NS} and ν_{K0} in GX 17+2 than in the other Z sources would of course also lead to a lower HBO frequency. However, in that situation the *range* in HBO frequency, which is determined by the range in ν_{K0} , would still be expected to be similar to that in the other sources, whereas it is lower: \sim 12 Hz in GX 17+2 versus \sim 35 Hz in GX 5–1 and Cyg X-2.

Since the maximum HBO frequency in GX 17+2 is about a factor of two lower than the maximum HBO frequency in Cyg X-2, GX 5–1 and GX 340+0, we now explore the possibility that the HBO frequency seen in GX 17+2 is dominated by the fundamental (first harmonic) of the field symmetry ($n=1$) and the HBO frequency seen in the latter sources by the second harmonic ($n=2$). This could be true if in GX 17+2 the radiation from one magnetic pole at the neutron star surface dominates that from the other magnetic pole, whereas in the other sources both poles contribute approximately the same amount of radiation. The less luminous magnetic pole in GX 17+2 is expected, if its luminosity is not negligible, to give rise to a second harmonic with centroid frequencies in a similar range as the HBO in the other sources, as actually observed in GX 17+2. The second harmonic seen in GX 5–1 and GX 340+0 is weak compared to that in GX 17+2 and in our interpretation due

to deviations of the HBO signal from being sinusoidal. If the above described model is right, we predict the presence of a subharmonic (due to the difference between the emission from the two poles) in the power spectra of GX 5–1, Cyg X-2 and GX 340+0, while it should be absent in the power spectra of GX 17+2.

Differences in the radiation from the two magnetic poles could be caused by asymmetries in the field geometry, which lead to different rates of accretion onto, or different emission characteristics from, the two poles. These asymmetries would also lead to a difference in the surface area of the two polar caps. Different polar cap areas have also been deduced from pulse analyses in several pulsars (e.g. Leahy 1991, Bulik et al. 1992).

We note that in a situation with unequal polar cap areas type I bursts might have a higher chance to occur, as on the larger of the two polar caps accretion per unit area would be less, and therefore on that pole the conditions for a type I burst would be more favourable than for two equal-area polar caps. The presence of bursts and the lower maximum HBO frequency might therefore be explained together in this model.

We shall for illustrative purposes consider one simple asymmetry in field geometry, namely that which arises when the (dipole) magnetic field center does not coincide with the neutron star center, but is shifted. In Figs. 8a and b we plotted a magnetic dipole field in which the neutron star center coincides with the magnetic field origin (Fig. 8a) and one in which the neutron star origin is somewhat shifted (Fig. 8b). In these figures we have indicated the polar caps as expected from the last closed field line in a simple dipole plus spherical magnetosphere geometry. It is known that deviations from this geometry will occur, especially near the inner disk edge, because of the magnetic field of the accretion disk (e.g. Ghosh & Lamb 1979, Spruit & Taam 1990), but we ignore this here. We computed the areas of the two polar caps by assuming magnetospheric radii between 15 and 100 km (which is roughly the range expected in Z sources, see Ghosh & Lamb [1992]), and offsets of the magnetosphere origin with respect to the neutron star origin between 0 and 5 km. The neutron star was assumed to have a radius of 10 km. In Table 6 we give the results. As can be seen in this table, a slight offset of the magnetic dipole has a large effect on the polar cap areas. The ratio of the two polar cap areas already exceeds 2 for offsets of only \sim 1.5 km. For small magnetospheric radii, a small offset will cause the larger of the two polar caps to cover a considerable fraction of its hemisphere.

When \dot{M} increases along the Z, the magnetospheric radius becomes smaller. This leads to a rapid increase in the polar cap areas, which might explain the fact that the four bursts observed with *EXOSAT* occurred in the NB and FB, and not in the (lower \dot{M}) HB. However, somewhat dependent on the inner disk model (see Ghosh & Lamb 1992), accretion per unit area is usually still expected to increase when total \dot{M} increases in our simple model, even on the larger of the two polar caps.

The presence of multipole components in the magnetic field is another possibility to cause the required asymmetries between the accretion regions. As multipole effects increase very strongly with decreasing radius, these effects would be most prominent for small magnetospheric radius, i.e., at

higher \dot{M} or for lower overall magnetic field strengths. An overall lower magnetic field in GX 17+2 (as suggested by Psaltis et al. 1995, see the discussion in Section 6.1) could also be the explanation of the occurrence of bursts in this source, and the increase of \dot{M} from HB towards NB might explain why no bursts have been found in the HB.

6.2.3 Flaring branch QPO

On one occasion we found evidence for FBO with a frequency, FWHM and rms amplitude of 16 Hz, 7 Hz and 2 per cent, respectively. Similar FBO in GX 17+2 were reported earlier in *Ginga* data by Penninx et al. (1990) with frequencies up to 20 Hz and rms up to 3 per cent, but not from *EXOSAT* data. Sco X-1 is the only other Z source for which similar FBO have been reported (see Dieters & van der Klis 1996, and references therein). This kind of FBO merges smoothly with the NBO, and therefore probably has a common origin. FBO, and the NBO, are believed to be due to oscillations in the optical depth of the radial flow in the inner disk region (Lamb 1989, Fortner, Lamb & Miller 1989) or due to sound waves in the thick accretion disk (Hasinger 1987b, Alpar et al. 1992).

It was recently suggested that the strength of the NBO oscillations depends on the inclination at which we view the Z sources (Kuulkers & van der Klis 1995), stronger NBO occurring in the lower-inclination sources. The strength of the NBO in the lower NB and the fact that we observe FBO in GX 17+2 are in accordance with this. It is not clear how this difference could be explained in the Psaltis et al. (1995) model for the two groups of Z sources.

6.2.4 High-frequency noise

We found that in GX 17+2 the strength of the HFN decreases as a function of S_Z from the HB to the middle part of the NB from ~ 5.3 per cent to ~ 2.5 per cent. From the middle part of the NB to the FB the HFN is more or less constant at a level of ~ 2.5 per cent. This is different from what is seen in Sco X-1 (Hertz et al. 1992, Dieters & van der Klis 1996), and probably Cyg X-2 (Hasinger et al. 1990, Hasinger 1993, private communication). There the HFN is reported to decrease from the HB, to the NB, *into* the FB. None of these observations were obtained with the *EXOSAT* ME argon detectors, as our observations. The results for Sco X-1 and Cyg X-2 from *Ginga* (Hertz et al. 1992, Hasinger et al. 1990, Hasinger 1993, private communication) indicated values which were typically lower than ~ 1.5 per cent in the FB. It has recently been suggested that some of the HFN seen with the *EXOSAT* ME is instrumental, up to an rms strength of ~ 2.3 per cent (0.01–100 Hz) in the argon data (Berger & van der Klis 1994, 1997). This instrumental effect has an amplitude similar to the values found in the middle part of the NB and FB of GX 17+2. We conclude that our data are therefore consistent with a decrease in HFN strength from the HB to the FB.

6.3 Bursts in GX 17+2

We have detected two bursts in GX 17+2 in the 1986 data. One burst was about 100 s long, the other (which occurred

~ 19 hr later) lasted ~ 300 s. Previously, Sztajno et al. (1986) had found two bursts in the 1984 and 1985 data of *EXOSAT*, which lasted ~ 10 and ~ 300 s, respectively. Bursts in this source have also been observed with other X-ray instruments: one with *Einstein* (~ 10 s, Kahn & Grindlay 1984) and four with *Hakucho* (two which lasted for ~ 100 s and two which lasted for ~ 300 s, Tawara et al. 1984). All bursts have large α values ($\alpha > 1000$) and γ larger than 1 (i.e., the net peak burst flux is smaller than the average persistent flux).

We found that the *EXOSAT* bursts occurred in the NB and lower part of the FB, i.e. at near-Eddington mass accretion rates. None were found in the HB, i.e. when \dot{M} is lowest, although we can not rule out the possibility that this is a coincidence. The only other Z source that has shown X-ray bursts is Cyg X-2 (Kahn & Grindlay 1984, Kuulkers et al. 1995, Wijnands et al. 1997, Smale et al. 1996). The occurrence of these bursts was found to be independent of branch position (Kuulkers et al. 1995, Wijnands et al. 1997).

Bildsten (1993, 1995) suggested that rotating patches of nuclear-burning material on the neutron star surface during X-ray bursts may produce regular pulsations (see also Schoelkopf & Kelley 1991). We searched for such pulsations in all four *EXOSAT* bursts, but found none, with upper limits to the modulation strength of ~ 1 per cent (if the signal is sinusoidal). A similar lack of pulsations was found for the persistent emission (Vaughan et al. 1994b) and in a large sample of X-ray bursts from other sources (Jongert & van der Klis 1996).

From the fact that the two new *EXOSAT* bursts show spectral softening during their evolution, we conclude that, like the bursts reported by Sztajno et al. (1986), they are type I X-ray bursts caused by thermonuclear flashes on the neutron star surface (Hoffman, Marshall & Lewin 1978, see also Lewin et al. 1993 and references therein). The bursts in Cyg X-2, although much weaker than those in GX 17+2, are also thought to be due to thermonuclear flashes, since the burst properties resemble those of type I bursts (see Kuulkers et al. 1995, Wijnands et al. 1997). However, no evidence for spectral softening was found. A burst recently detected with RXTE in Cyg X-2 (Smale et al. 1996) is the first case of a bona fide type I burst in this source. The fact that two Z sources show type I bursts indicates that the compact star in systems of this type is a neutron star.

High luminosity burst sources tend to show irregular bursting behaviour (Van Paradijs et al. 1988b). They show bursts after long and variable waiting times. This is most probably due to steady nuclear burning, which occurs at high mass accretion rate \dot{M} . It is unlikely that \dot{M} is lower in GX 17+2 and Cyg X-2 as compared with the other Z sources, as in the NB \dot{M} is believed to be approximately Eddington in all Z sources (Lamb 1989). If bursts do apparently occur at these high levels of \dot{M} (see e.g. Taam, Woosley & Lamb 1996), then it is not clear why bursts are not seen in the other Z sources as well. From the presence of HBO in Z sources one derives that they contain a neutron star with a non-negligible magnetic field. In Section 6.2.2 we have discussed the possibility that the magnetic field strength might affect the probability to produce bursts in a Z source.

7 SUMMARY

We found that the position of the Z pattern in the CD is not moving by more than a few percent between observations separated by from 1 day up to ~ 1.5 years. This is in accordance with the division of the Z sources in two groups, in which the Cyg-like sources (GX 5-1, Cyg X-2 and GX 340+0) show secular variations in their Z pattern in the CD, while the Sco-like sources (GX 17+2, Sco X-1 and GX 349+2) do not.

We have investigated the various power spectral components as a function of position in the Z, S_Z , and placed their properties in the framework of the division of Z sources into two groups and discussed the hypothesis that this division is due to differences in viewing geometry. Many, but not all, source properties fit in this picture.

Two new X-ray bursts were found in GX 17+2 lasting ~ 100 and ~ 300 s, which came at an interval of ~ 19 hr. These bursts, and also those seen by Sztajno et al. (1986), occurred in the NB or in the lower part of the FB, i.e. presumably near Eddington accretion rates. No evidence for regular pulsations was found in the bursts.

We suggest that an asymmetric magnetic field, giving rise to different surface areas and emission characteristics of the magnetic pole areas at the neutron star surface may simultaneously explain the occurrence of bursts in GX 17+2, the fact that they were not seen at the lowest accretion rates, the fact that the maximum HBO frequency in GX 17+2 is lower by about a factor two than the maximum HBO frequency in Cyg X-2, GX 5-1 and GX 340+0 near the HB/NB apex, and the fact that the observed range in HBO frequency in GX 17+2 is about a factor of two smaller than that of Cyg X-2 and GX 5-1. The asymmetry could for example be due to an overall lower field strength, allowing the multipole component of the magnetic field to play a larger role due to the smaller radius of the atmosphere.

ACKNOWLEDGEMENTS

Stefan Dieters is gratefully acknowledged for his discussions. We also thank him and Frank Verbunt for comments on earlier versions of this paper. This work was supported in part by the Netherlands Organization for Scientific Research (NWO) under grant PGS 78-277. WHGL acknowledges support from NASA.

REFERENCES

Alpar M. A., Shaham J., 1985, *Nat*, 316, 239
 Alpar M. A., Hasinger G., Shaham J., Yancopoulos S., 1992, *A&A*, 257, 627
 Andrews D., 1984, *EXOSAT Express*, 5, 31
 Andrews D., Stella L., 1985, *EXOSAT Express*, 10, 35
 Berger M., van der Klis M., 1994, *A&A*, 292, 175
 Berger M., van der Klis M., 1997, *A&A*, submitted
 Bildsten L., 1993, *ApJ*, 418, L21
 Bildsten L., 1995, *ApJ*, 438, 852
 Bulik T., Mészáros P., Woo J. W., Nagase F., Makeshima K., 1992, *ApJ*, 395, 564
 Cowley A. P., Crampton D., Hutchings J. B., 1979, *ApJ*, 231, 539
 Crampton D., Cowley A. P., Hutchings J. B., Kaat C., 1976, *ApJ*, 207, 907
 Deeter J. E., 1984, *ApJ*, 281, 482
 Dieters S., van der Klis M., 1997, *MNRAS*, submitted
 Focke W.B., 1997, *ApJ*, 470, L127
 Fortner B., Lamb F. K., Miller G. S., 1989, *Nat*, 342, 775
 Ghosh P., Lamb F. K., 1979, *ApJ* 234, 296
 Ghosh P., Lamb F. K., 1992, in van den Heuvel E. P. J., Rappaport S. A., eds, *Proc. NATO Conf. on X-ray Binaries and Recycled Pulsars*. Kluwer, Dordrecht, p. 487
 Hasinger G., 1987a, in Helfand D. J., Huang J.-H., eds, *IAU Symp. 125, The Origin and Evolution of Neutron Stars*. Kluwer, Dordrecht, p. 333
 Hasinger G., 1987b, *A&A*, 186, 153
 Hasinger G., Priedhorsky W.C., Middleditch J., 1989, *ApJ*, 337, 843
 Hasinger G., van der Klis M., 1989, *A&A*, 225, 79
 Hasinger G., van der Klis M., Ebisawa K., Dotani T., Mitsuda K., 1990, *A&A*, 235, 131
 Hertz P., Vaughan B., Wood K. S., Norris J. P., Mitsuda K., Michelson K. P., Dotani T., 1992, *ApJ*, 396, 201
 Hoffman J. A., Marshall H. L., Lewin W. H. G., 1978, *Nat*, 271, 630
 Jongert H., van der Klis M., 1996, *A&A*, 310, 474
 Kahn S. M., Grindlay J. E., 1984, *ApJ*, 281, 826
 Kuulkers E., 1995, PhD thesis, University of Amsterdam
 Kuulkers E., van der Klis M., 1995, *A&A*, 303, 801
 Kuulkers E., van der Klis M., 1996, *A&A*, 314, 567
 Kuulkers E., van der Klis M., Oosterbroek T., Asai K., Dotani T., Van Paradijs J., Lewin W. H. G., 1994a, *A&A*, 289, 795
 Kuulkers E., van der Klis M., Oosterbroek T., Van Paradijs J., Lewin W. H. G., 1994b, in Holt S. S., Day C. S., eds, *The Evolution of X-ray Binaries*. American Institute of Physics, p. 539
 Kuulkers E., van der Klis M., Van Paradijs J., 1995, *ApJ*, 450, 748
 Kuulkers E., van der Klis M., Vaughan B. A., 1996, *A&A*, 311, 197
 Lamb F. K., 1989, Hunt J., Battrick B., eds, *23rd ESLAB Symp. on Two-Topics in X-ray Astronomy: X-ray Binaries*. ESA SP-296, p. 215
 Lamb F. K., Shibasaki N., Shaham J., Alpar M. A., 1985, *Nat*, 317, 681
 Langmeier A., Hasinger G., Trümper J., 1990, *A&A*, 228, 89
 Langmeier A., Sztajno M., Vacca W. D., Trümper J., Pietsch W., 1986, in Trümper J. et al., eds, *The Evolution of Galactic X-ray Binaries*. D. Reidel Publishing Company, p. 253
 Leahy D. A., 1991, *MNRAS*, 251, 203
 Leahy D. A., Darbrow W., Elsner R., Weisskopf M. C., Sutherland P. G., Kahn S., Grindlay J. E., 1983, *ApJ*, 266, 160
 Lewin W. H. G., Lubin L. M., Tan J., van der Klis M., Van Paradijs J., Penninx W., Dotani T., Mitsuda K., 1992, *MNRAS*, 256, 545
 Lewin W. H. G., Van Paradijs J., Taam R. E., 1993, *Sp. Sc. Rev.*, 62, 223
 Lewin W. H. G., Van Paradijs J., van der Klis M., 1988, *Sp. Sc. Rev.*, 46, 273
 Penninx W., Lewin W. H. G., Mitsuda K., van der Klis M., Van Paradijs J., Zijlstra A. A., 1990, *MNRAS*, 243, 114
 Penninx W., Lewin W. H. G., Tan J., Van Paradijs J., van der Klis M., Mitsuda K., 1991, *MNRAS*, 249, 113
 Psaltis D., Lamb, F.K., Miller G.S., 1995, *ApJ*, 454, L137
 Schoelkopf R. J., Kelley R. L., 1991, *ApJ*, 375, 696
 Schulz N. S., Hasinger G., Trümper J., 1989, *A&A*, 225, 48
 Smale A. P., et al., 1996, in preparation
 Spruit H. C., Taam R. E., 1990, *A&A*, 229, 475
 Stella L., Parmar A. N., White N. E., 1987, *ApJ*, 321, 418
 Sztajno M., Van Paradijs J., Lewin W. H. G., Langmeier A., Trümper J., Pietsch W., 1986, *MNRAS*, 222, 499
 Taam R. E., Woosley S. E., Lamb D. Q., 1996, *ApJ* 459, 271

Tawara Y., Hirano T., Kii T., Matsuoka M., Murakami T., 1984, PASP, 96, 861

Tennant A. F., 1987, MNRAS, 226, 963

Turner M. J. L., Smith A., Zimmerman H. U., 1981, Sp. Sci. Rev., 30, 513

van der Klis M., 1989, in Ögelman H., van den Heuvel E. P. J., eds, Timing Neutron Stars. Kluwer, Dordrecht, p. 27

van der Klis M., 1994, ApJS, 92, 511

van der Klis M., Stella L., White N., Jansen F., Parmar A. N., 1987, ApJ, 316, 411

van der Klis M., Swank J. H., Zhang W., Jahoda K., Morgan E. H., Lewin W. H. G., Vaughan B., Van Paradijs J., 1996, ApJ, 469, L1

Van Paradijs J., Hasinger G., Lewin W. H. G., van der Klis M., Sztajno M., Schulz N., Jansen F., 1988, MNRAS, 231, 379

Van Paradijs J., Penninx W., Lewin W. H. G., Sztajno M., Trümper J., 1988, A&A, 192, 147

Vaughan B. A., van der Klis M., Wood K. S., Norris J. P., Hertz P., Michelson P. F., Van Paradijs J., Lewin W. H. G., Mitsuda K., Penninx W., 1994, ApJ, 435, 362

White N., 1986, EXOSAT Express, 16, 2

White N. E., Peacock A., 1988, Mem. S. A. It., 59, 7

Wijnands R. A. D., Kuulkers E., Smale A. P., 1996b, ApJ, 473, L45

Wijnands R. A. D., van der Klis M., Kuulkers E., Asai K., Hasinger G., 1997, A&A, in press

Wijnands R. A. D., van der Klis M., Psaltis D., Lamb F. K., Kuulkers E., Dieters S., Van Paradijs J., Lewin W. H. G., 1996a, ApJ, 469, L5

APPENDIX A: DEAD TIME AND POISSON NOISE

Dead time is a severe problem in X-ray astronomy (e.g. Lewin, Van Paradijs & van der Klis 1988, van der Klis 1989). Once an X-ray photon is detected, the detector remains “dead” for a certain or variable time. During this “dead time” the detector is unable to register new incoming X-ray photons. The various dead time processes onboard *EXOSAT* have been described by Andrews (1984), Andrews & Stella (1985) and Tennant (1987). When the detector is dead for a fixed amount of time after a photon has been detected, one speaks of a fixed dead time. In the case the detector can only register one photon within a given time (or “sample cycle”), the dead time is variable (i.e. depending on where the photon is detected within the sample cycle), and one speaks in terms of variable dead time. Within the ME instrument (i.e. the detector, electronics and the OBC) both constant dead time (in non-OBC processed data, such as HTR3 and HTR5 observation modes) and variable dead time (in HTR4 and all HER observation OBC modes) processes occur (Andrews 1984, Andrews & Stella 1985, Tennant 1987, Berger & van der Klis 1994).

Dead time processes have recognizable effects on power spectra (see Lewin et al. 1988, van der Klis 1989). Pure counting noise, in the absence of dead time, has a white power spectrum with, in the case of the Leahy et al. (1983) normalization, an average power of two. This white noise component is called Poisson noise and its level the Poisson level. The Poisson level is modified by the dead time process. The larger the dead time, the lower the Poisson level. Also the dead-time modified Poisson noise is not necessarily white any more. The effect of the fixed dead time of HTR3 and

HTR5 on the power spectrum has been studied by Berger & van der Klis (1994, 1997).

In the case of variable dead time, the Poisson level is approximated as follows (e.g. van der Klis 1989):

$$P_{\text{Poiss}} = 2(1 - \mu\tau_{\text{sample}}), \quad (\text{A1})$$

where τ_{sample} is the duration of the sample cycle, and μ the observed count rate. For the *EXOSAT* ME value of τ_{sample} , 1/4096 s, this expression gives wrong results. For a so-called effective sampling time of 1/3569 s (Andrews & Stella 1985) an approximate match with the data is found.

Recently we found (Kuulkers et al. 1994a) that for high observed count rates (1500–2300 cts s^{-1}) in the OBC processed HER7 data the fitted Poisson levels deviated from that expected from Eq. A1. Since the HER7 data of GX 17+2 provided lower count rates (0–1500 cts s^{-1}), we decided to analyse all four-channel HER7 data for the brightest LMXBs, i.e. Sco X-1, GX 5-1, Cyg X-2, GX 17+2 and GX 3+1. The former four sources are all Z sources, while the latter is an atoll source (see e.g. Hasinger & van der Klis 1989). In Table A1, we give an observation log of the four channel HER7 argon observations of these sources. We selected the power spectra according to observed intensity and determined the Poisson level by fitting the power spectra with the various source components as described in Section 3, with the Poisson level as a free parameter. This was done for each source individually. The results are given in Fig. A1. In this figure we also plotted the Poisson levels as predicted from the linear relation Eq. A1. It is clear that the fitted Poisson levels deviate from those expected (especially at high count rates), as was already found by Kuulkers et al. (1994a). It can be seen that the Poisson level deviations from the predicted linear relation in the various sources where they overlap are the same. The deviation is therefore not an effect related to variability in the sources themselves.

As mentioned in Section 3, we rebinned the OBC processed HTR4 data to a time resolution of ~ 4 ms, i.e. similar to most of the HER7 data. In the power spectral fits of the HTR4 data the Poisson level was also taken to be a free parameter. The results of these Poisson level fits are also plotted in Fig. A1. As can be seen in this figure, the HTR4 data fall along the HER7 data points, as expected from the fact that these data are processed in a similar way, by the OBC, to the HER7 data.

Although a linear deviation was sufficient to describe the GX 5-1 data of Kuulkers et al. (1994a), they noted that the Poisson level could be better described as a quadratic function of observed intensity. Here we find that a linear fit is unacceptable, and that our data are described by a quadratic function. When fitting the data to such a function, the Poisson level as a function of observed intensity, μ , is as follows:

$$P_{\text{Poiss HER7}} = 1.9959(19) - 5.89(4) \cdot 10^{-4} \mu + 3.04(13) \cdot 10^{-8} \mu^2, \quad (\text{A2})$$

where we give the uncertainty in the last digit(s) in brackets. The fitted Poisson levels in the observed count rate range 100–900 cts s^{-1} are below the expected Poisson levels. This is consistent with a previous study by Rutledge (1993 private communication) from HER7 data of the Rapid Burster.

We note that it was possible to fit the following function to the data:

$$P_{\text{Poiss HER7}} = 2 \left(1 + \sum_{i=0}^n (-1)^i \frac{1}{i^2} (\mu \tau_{\text{sample}})^i \right). \quad (\text{A3})$$

We found that χ^2_{red} was ~ 1.0 for $n=4$. In that case τ_{sample} was found to be 1/3304 s.

Figure Captions

Figure 1:

(a) *EXOSAT* X-ray colour-colour diagram and (b, c) hardness-intensity diagrams of GX 17+2. Soft colour is defined as the ratio of the count rates in the 4.7–6.6 keV and the 1.2–4.7 keV bands, hard colour as the ratio of the counts in the 6.6–19.9 keV and the 4.7–6.6 keV bands. The intensity (corrected for background, dead-time and collimator response) is defined as the count rate in the 1.2–19.9 keV band. Different symbols refer to different observation periods, which are given in the lower right part of (a). Each point represents a 200 s average. Typical error bars are given in each frame. HB (horizontal branch), NB (normal branch) and FB (flaring branch) are indicated. In a we give the position in the CD at the time the different bursts (1984 day 250: I, 1985 day 232: II, 1986 day 093: III, 1986 day 094: IV) occurred (see Section 5.2).

Figure 2:

(a) Colour-colour diagram and (b, c) hardness-intensity diagrams of GX 17+2 of the 1983 data. The colours and intensity are as defined in Fig. 1. The points are connected to show more clearly the different branches, which are indicated. Each point represents a 200 s average.

Figure 3:

Three examples of average power spectra corresponding to different segments in S_Z . The corresponding fits are shown for clarity, and the power spectral components are indicated. (a) Power spectra for data of 1985 day 258/259 when GX 17+2 was in the upper part of the HB near $S_Z \sim 0.1$. Both the HBO and its harmonic can be seen, as well as the peaked noise component LFN. (b) Power spectra for data of 1985 day 232/233 during the NB near $S_Z \sim 1.8$. The NBO can be seen near 7.6 Hz. (c) Power spectra for data in the lower part of the FB during 1986 day 093/094 near $S_Z \sim 2.4$. The FBO can be seen near 16 Hz.

Figure 4:

(a)–(l) Properties of the various power spectral components as a function of position on the “Z”, S_Z . The different symbols refer to different observation periods as indicated in Fig. 1a. The 1983 day 215 data are indicated with \bigcirc . The boundaries between the spectral branches are indicated. (a) VLFN rms 512 s FFTs, (b) VLFN power law index 512 s FFTs, (c) VLFN rms 16 s FFTs, (d) VLFN power law index 16 s FFTs, (e) LFN rms 16 s FFTs, (f) LFN power law index 16 s FFTs, (g) LFN cut-off frequency 16 s FFTs, (h) HFN rms 512 s FFTs, (i) HFN cut-off frequency 512 s FFTs, (j) NBO frequency, (k) NBO rms (l) NBO FWHM.

Figure 5:

EXOSAT ME light curves of 4 observation periods of GX 17+2 at a time resolution of 5 s. Intensity is the dead-time-, background- and collimator-response-corrected count rate in the 1.2–19.9 keV range. Indicated are the branches in which the source was during the observations. During two observation periods (1984 day 251/250, [c], and 1985 day 232/233, [d]) bursts can be seen which were already reported by Sztajno et al. (1986). Start times for the different observation periods can be found in Table 1.

Figure 6:

EXOSAT ME light curve (a) and soft colour curve (b) of the observation period 1986 day 093/094. Intensity is the dead-time and background corrected count rate in the 1.2–19.9 keV range, while the soft colour is the ratio of the count rate in the 4.7–6.6 keV and the count rate in the 1.2–4.7 keV band. The intensities are not corrected for collimator response (see text). Two new bursts can be seen at ($\sim 36\,000$ and $\sim 104\,000$ s after the start of the observation). The start time of the observation period can be found in Table 1.

Figure 7:

High time resolution (0.5 s) argon light curves of the bursts which occurred during 1986 day 093 (a) and 1986 day 094 (b), together with their colour (ratio of the count rates in the 4.7–19.9 keV and 1.2–4.7 keV bands) curves, [c] and [d], respectively. During the 1986 day 094 burst the observations were interrupted for mode changes. The qualified event rate from the housekeeping data is therefore also plotted in b (with symbol \bigcirc) to show the overall burst profile.

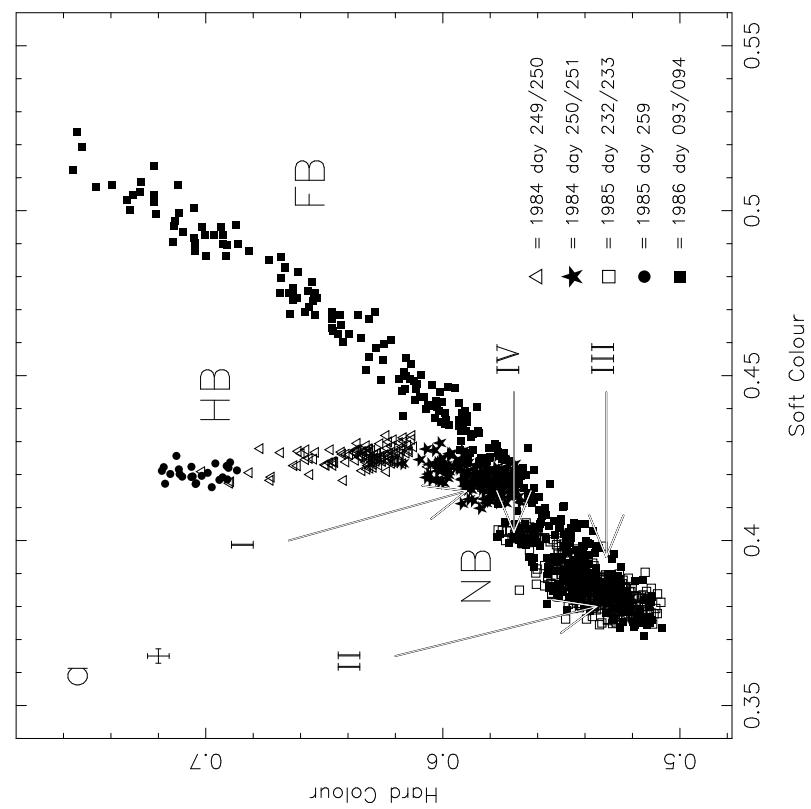
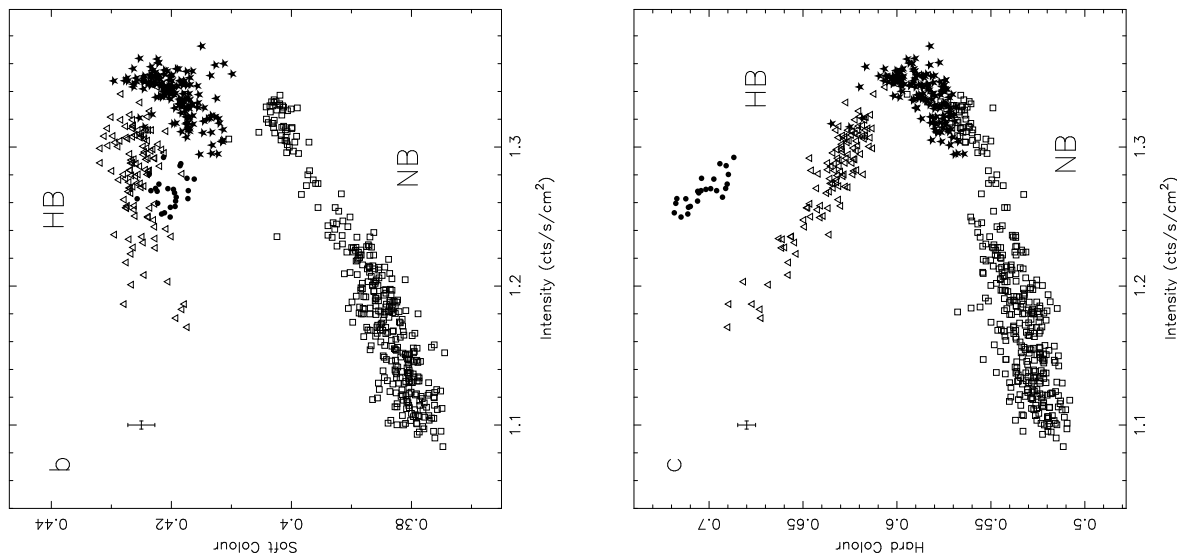
Figure 8:

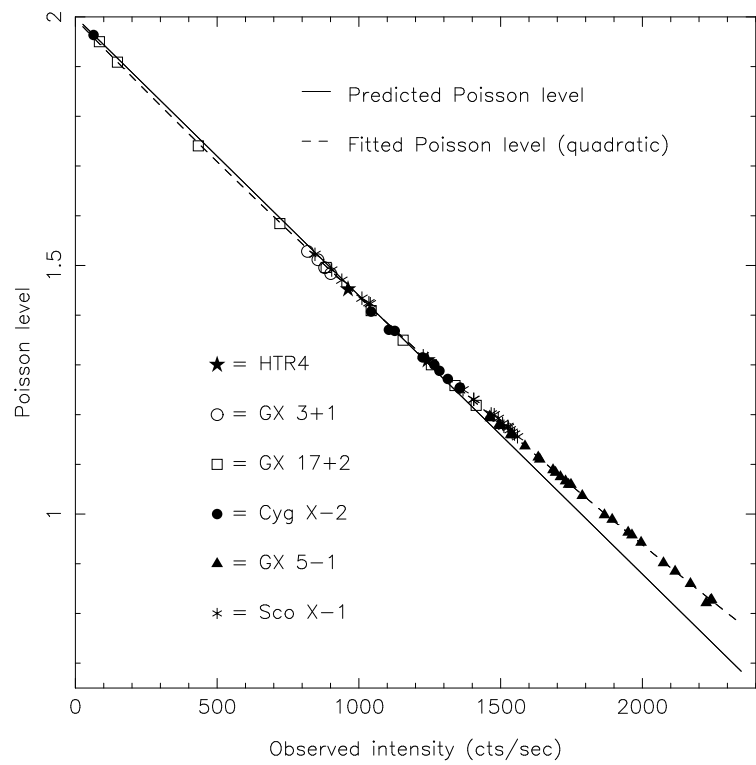
(a) A neutron star (radius 10 km) with a symmetric dipole field. The spherical magnetosphere (indicated by a dotted line) in this plot is taken to be at a radius of 30 km. The last closed field line is indicated with a dashed line. The corresponding accretion polar cap on the surface of the neutron star is indicated with a fat line. (b) Same neutron star with a shifted (by 5 km) magnetic dipole field. The upper pole now has a much larger area than the lower pole.

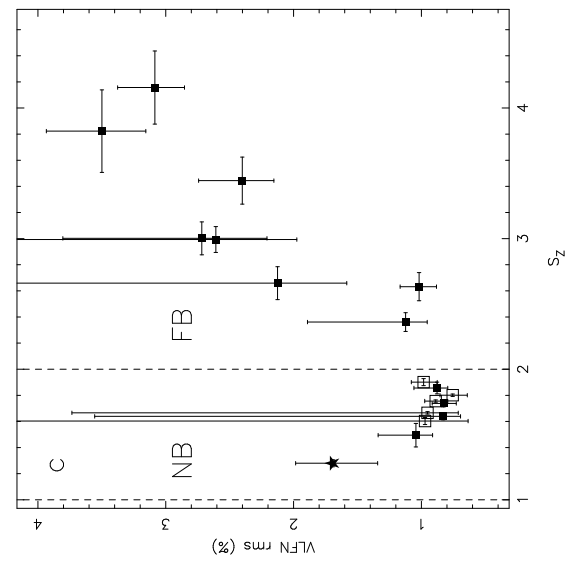
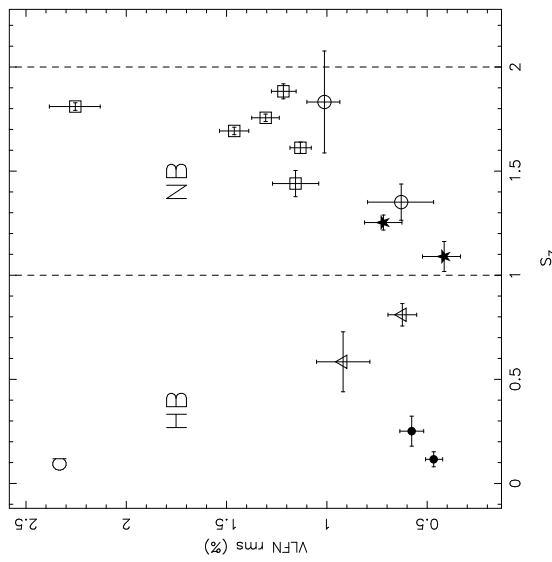
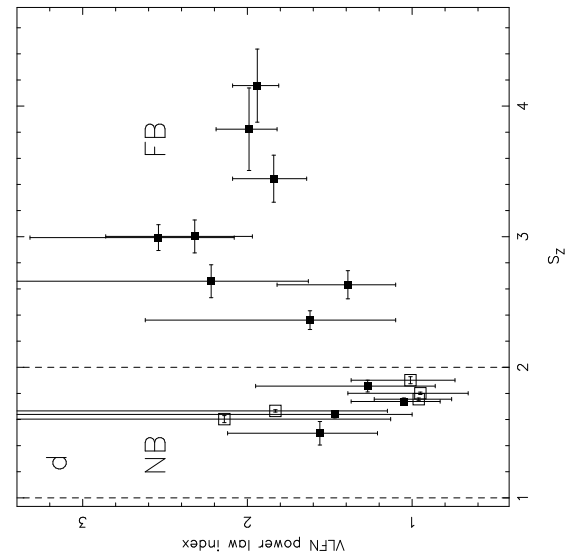
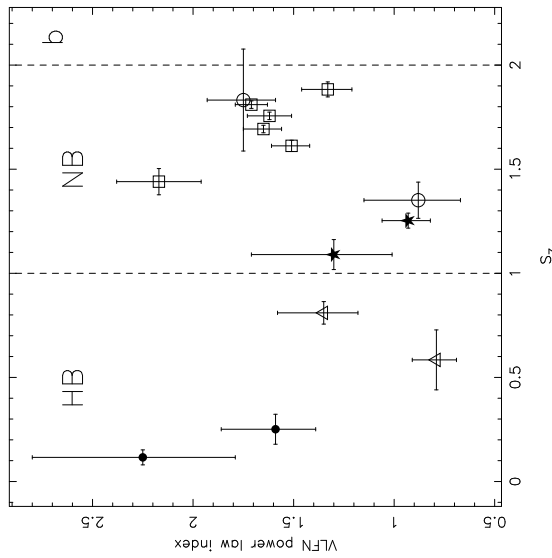
Figure A1:

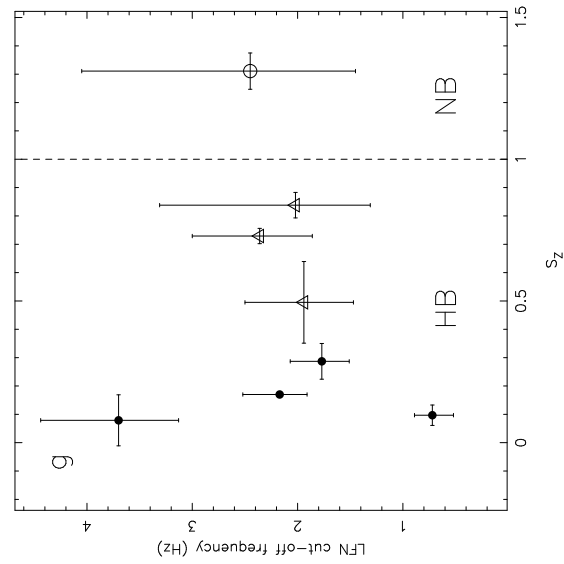
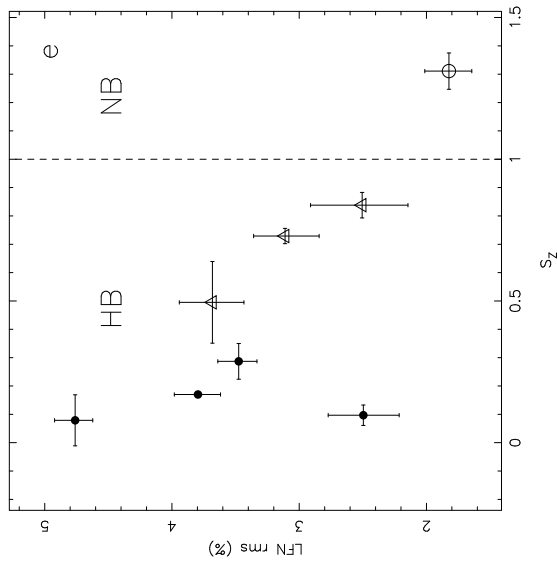
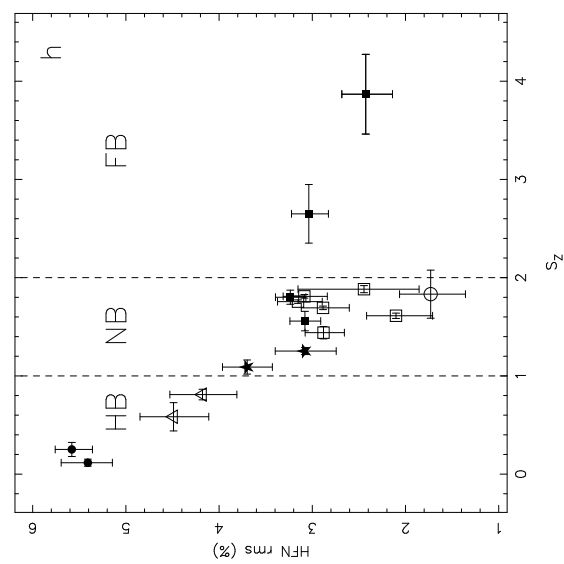
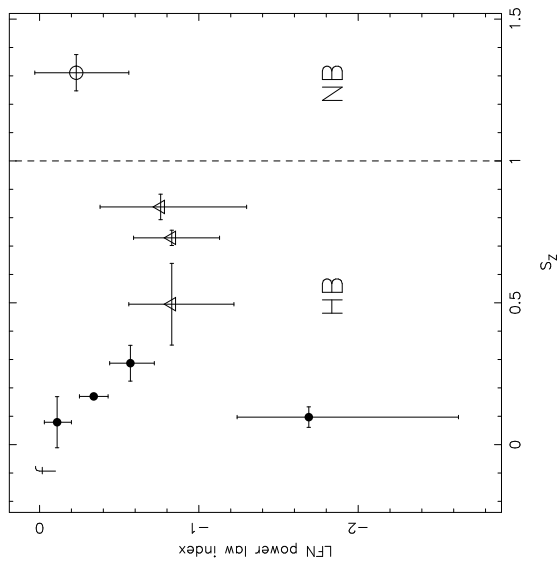
Observed Poisson levels for the power spectra of HER7 data for several LMXBs as a function of the raw observed count rate. The HTR4 data of GX 17+2 have also been plotted. The observed Poisson level was determined by adding it as an extra component in the power spectral fits. The different symbols refer to the different sources as indicated. Error bars are on the order of the symbol sizes. The predicted Poisson levels (straight line) and the quadratic fit (dashed line) are included in the plot.

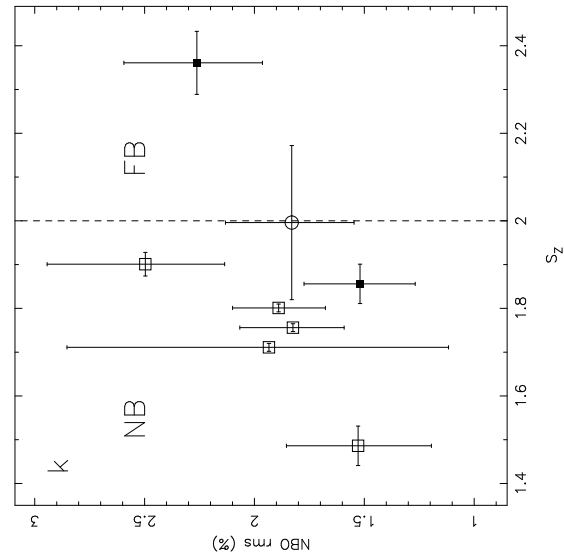
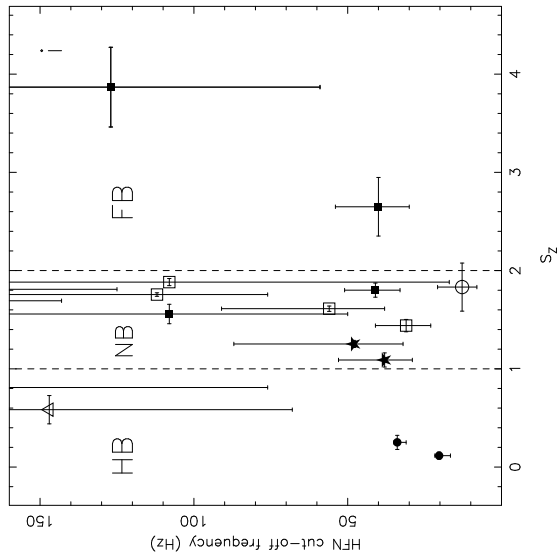
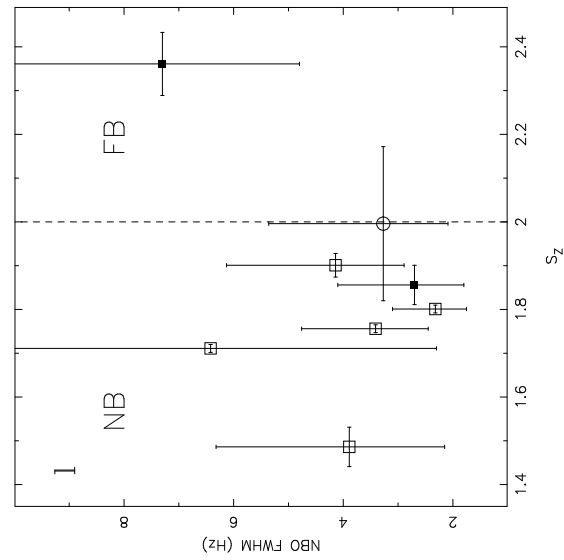
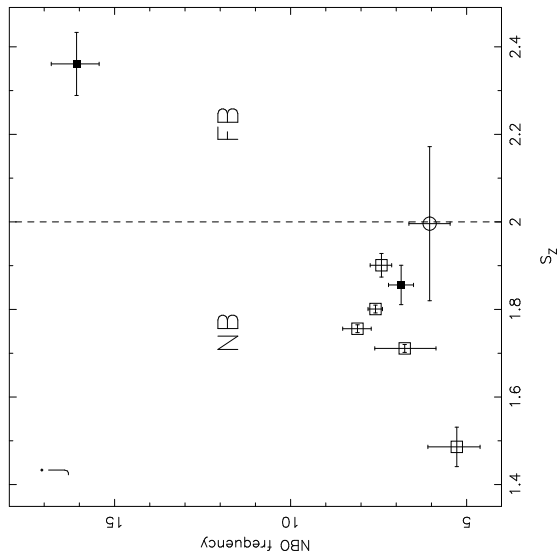
This paper has been produced using the Royal Astronomical Society/Blackwell Science L^AT_EX style file.

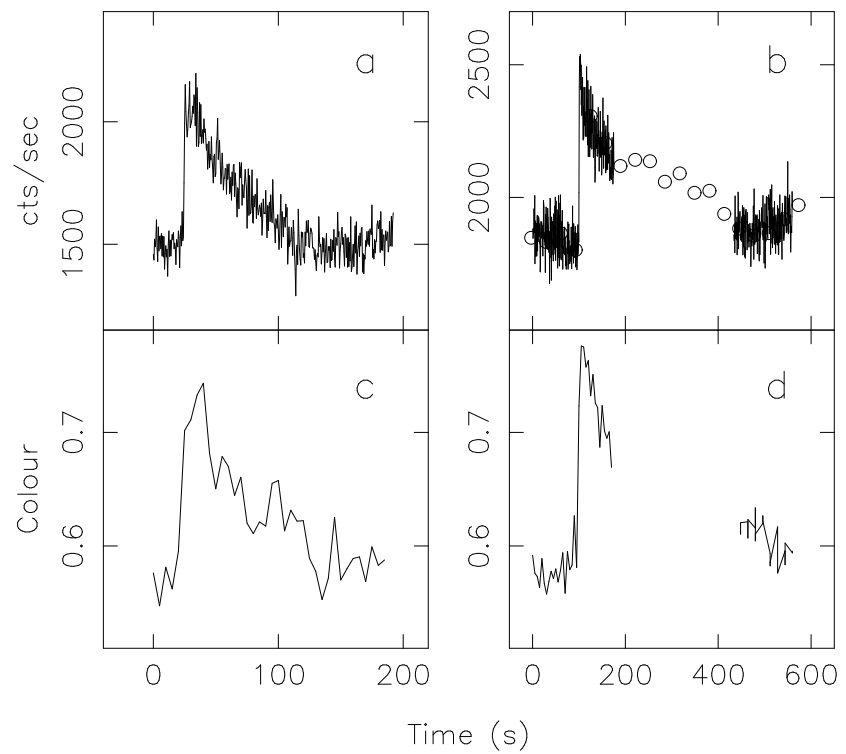


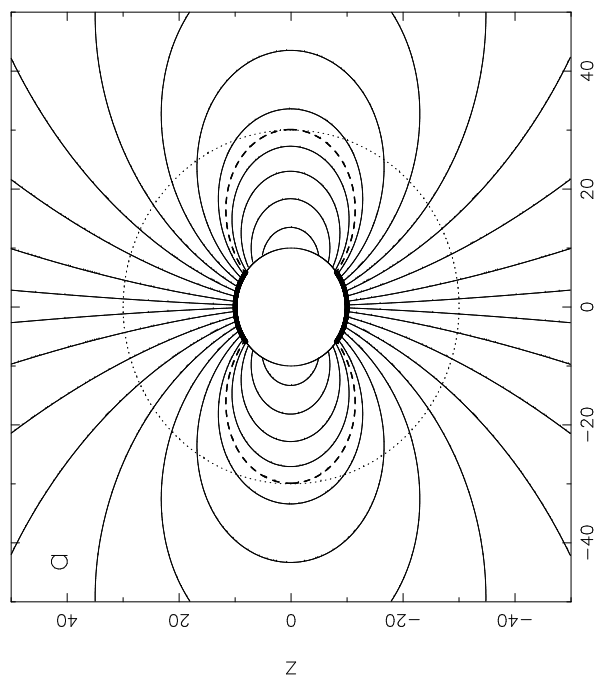
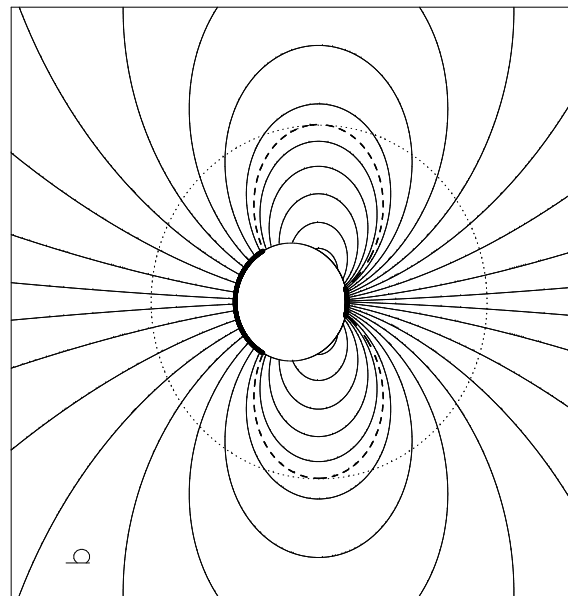


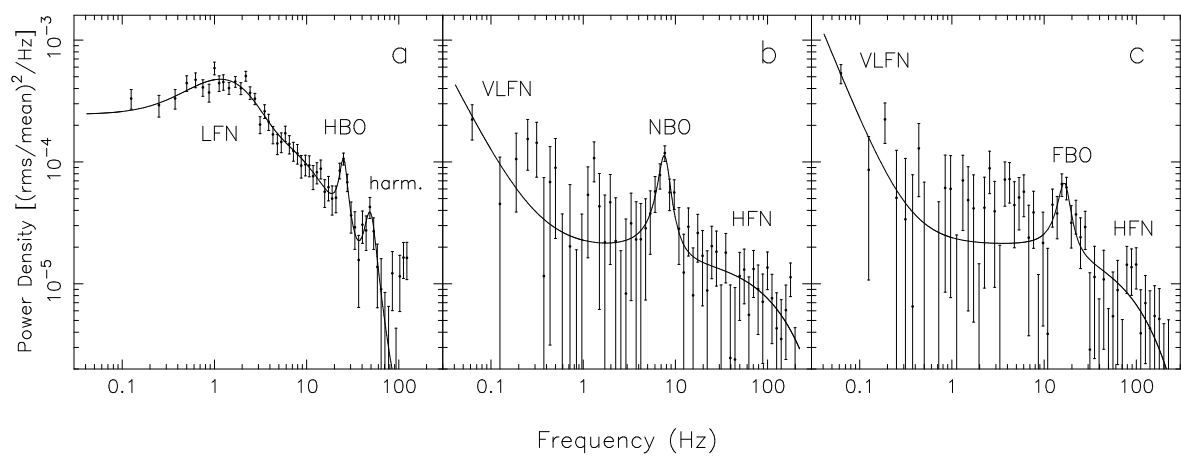
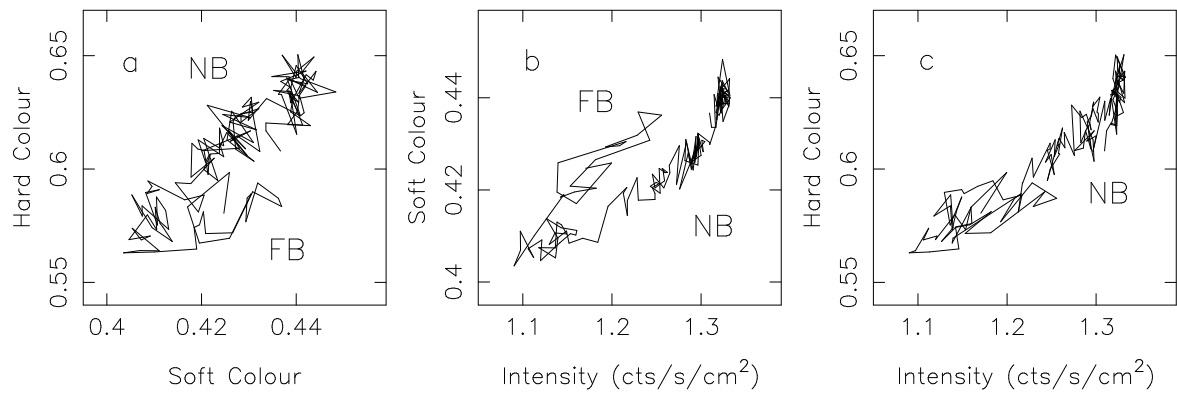












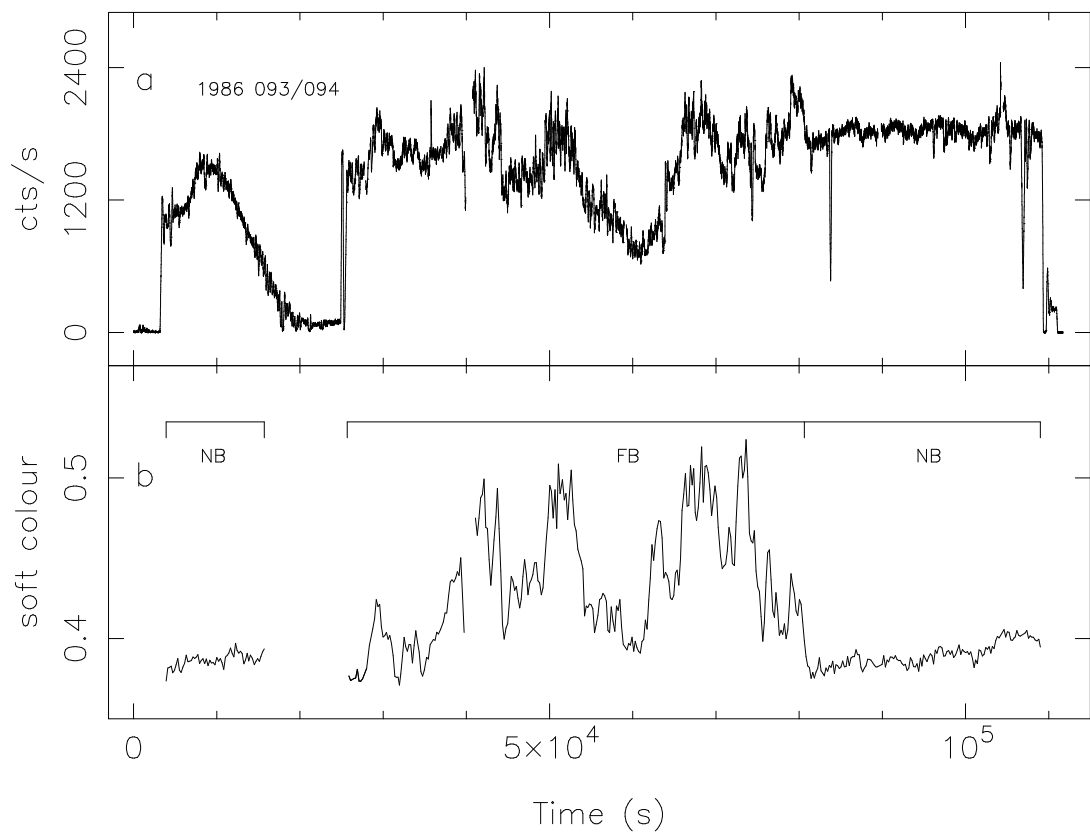
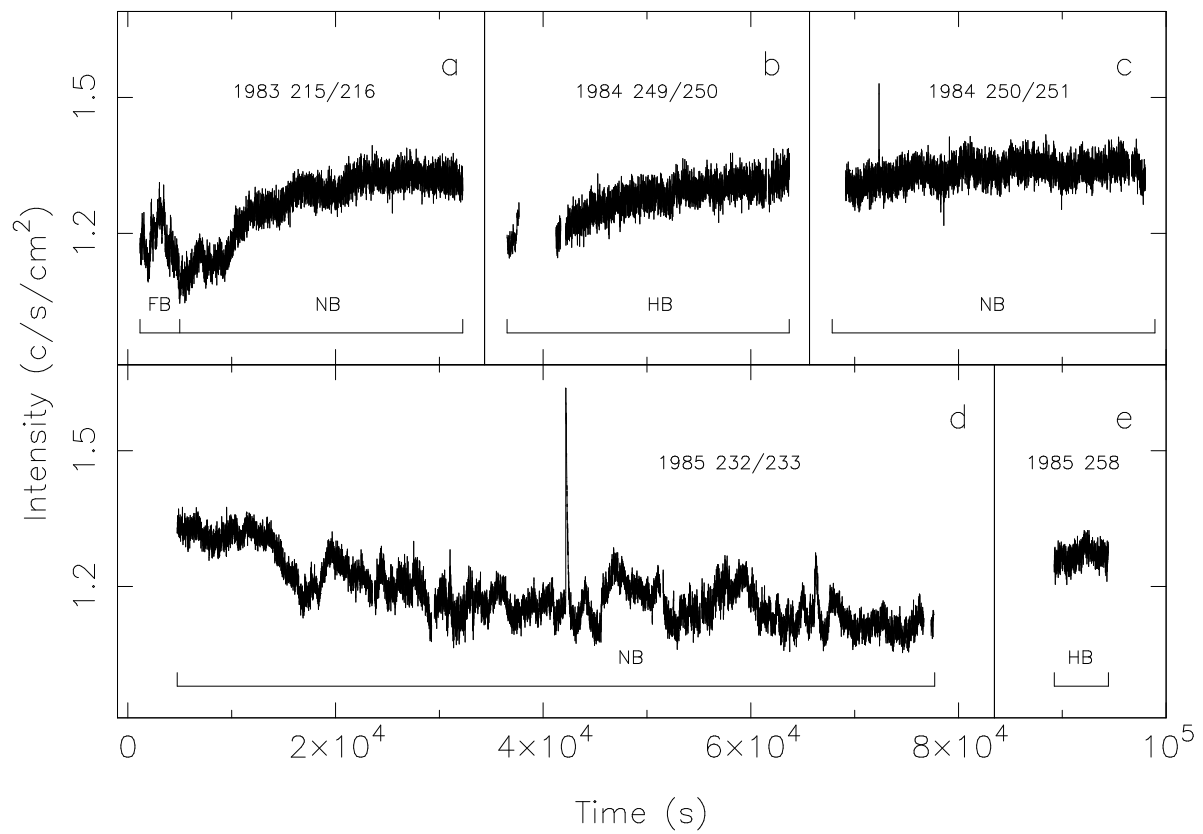


Table 1: EXOSAT Argon observation log of GX 17+2

Year	Date	Day ^a	UT start (hr:min)	UT end (hr:min)	Mode ^b	Time Resolution	Spectral State	Config. ^c
1983	Aug 3/4	215/216	15:58	00:36	E4/T3	0.3 s/8 ms	NB/FB	H2
1984	Sep 5/6	249/250	21:47	05:21	E4/5/T3 ^d	10/0.6 s/8 ms	HB	H1/H2 ^d
1984	Sep 6/7	250/251	19:42	04:04	E5/T3	0.6 s/8 ms	NB	H1/H2 ^e
1985	Aug 20/21	232/233	10:32	07:19	E5/T3	1 s/2 ms	NB	H1/H2/WA ^f
1985	Sep 15/16	258/259	16:15	04:48	E5/7/T3/4 ^g	0.7 s/2/4/0.25 ms	HB	WA
1986	Apr 3/4	093/094	04:09	11:10	E2/5/7/T4/5 ^h	1.4/1 s/8/0.25/1 ms	NB/FB	WA

^a Jan 1 = day 1.^b E = HER mode = High Energy Resolution mode, T = HTR mode = High Time Resolution mode.^c Array configuration on source: H1='half 1', H2='half 2', WA=whole array.^d From 21:47 to 22:07 HER4 (H1) the rest HER5/HTR3 (H2).^e From 19:41 to 19:51 H1; the rest H2.^f WA: 10:32 – 16:18, 19:02 – 00:03, 01:52 – 07:19; H2: 16:21 – 17:53, 00:01 – 01:04; H1: 17:57 – 19:02, 01:06 – 01:51.^g From 16:15 to 03:13 HER7/HTR3 (HER7 effectively one energy band: 1.4–4.1 keV; HTR3: from 16:15 to 22:58 xenon; the rest argon); the rest HER5/HTR4.^h HER2: day 093 15:28–20:31 (1 s) and day 093 22:55–day 094 09:07 (4 s); HER5: day 094 09:11–11:10;

HER7: day 093 04:09–15:14 and day 093 20:36–day 094 09:07; HTR4: day 093 15:25–20:31;

HTR5: day 093 04:09–15:14 and day 093 20:39–day 094 11:10.

Table 4: HBO harmonic parameters^a

Obs. period	\overline{S}_Z	σ_{S_Z}	harmonic						$\frac{rms_H}{rms_Q}c$	err	$\frac{\Delta\nu_H}{\Delta\nu_Q}d$	err
			rms	err ^b	$\Delta\nu$	err	ν	err				
			(%)		(Hz)		(Hz)					
512 s FFTs												
1985	0.116	0.036	2.1	± 0.5	8	± 3	49.2	± 0.5	1.1	± 0.3	3.0	± 1.4
day 258	0.251	0.072	1.3	± 0.4	4	± 2	52.1	± 1.0	0.8	± 0.3	1.4	± 0.9
1985	1.440	0.063	1.2	—	5	—	60	—	—	—	—	—
day 232	1.612	0.027	0.5	—	5	—	60	—	—	—	—	—
	1.693	0.018	0.6	—	5	—	60	—	—	—	—	—
1986	1.558	0.099	1.1	—	5	—	60	—	—	—	—	—
day 093												
16 s FFTs												
1985	1.386	0.027	1.6	—	5	—	60	—	—	—	—	—
day 232	1.486	0.045	0.6	—	5	—	60	—	—	—	—	—
	1.603	0.027	1.0	—	5	—	60	—	—	—	—	—
	1.666	0.009	1.0	—	5	—	60	—	—	—	—	—
	1.711	0.009	0.8	—	5	—	60	—	—	—	—	—
1985	0.097	0.036	3.0	± 0.4	16	± 6	49	± 2	1.1	± 0.2	2.9	± 1.3
day 258	0.170	0.009	1.4	—	6	—	52.6	—	0.9	—	—	—
	0.287	0.063	1.3	—	6	—	54.6	—	0.9	—	—	—
HTR4 ^{e,f}	0.079	0.090	2.5	± 0.6	10	± 8	52	± 2	0.7	± 0.2	1.5	± 1.3
1986	1.495	0.090	1.3	—	5	—	60	—	—	—	—	—
day 093	1.639	0.027	1.2	—	5	—	60	—	—	—	—	—
	1.738	0.027	0.6	—	5	—	60	—	—	—	—	—

^a Whenever a parameter was fixed or not evaluated it is indicated by “—” or “- -”, respectively.^b All errors in the power spectral parameters are determined from an error scan through the χ^2 space using $\Delta\chi^2 = 1$. If no error is given the parameter value is a 1σ upper limit.^c Ratio of the harmonic rms (rms_H) and the HBO rms (rms_Q).^d Ratio of the harmonic FWHM ($\Delta\nu_H$) and the HBO FWHM ($\Delta\nu_Q$).^e The Poisson level was a free parameter in the fits to these data.^f Effective energy range: 1.4–11.5 keV.

Table 2: Results of power spectral fits of 512 s FFTs^a

Obs. period	\overline{S}_Z	σ_{S_Z}	VLFN				LFN				HFN				QPO ^b				χ^2_{red}	dof				
			rms	err ^c	α_V	err	rms	err	α_L	err	ν_L (Hz)	rms	err	ν_H (Hz)	err	rms	err	$\Delta\nu$ (Hz)	err	ν (Hz)	err			
1983 day 215	1.351	0.087	0.63	± 0.16	0.88	± 0.24	1.5	± 0.3	-0.9	± 0.7	1.2	± 0.9	1.0	77	—	0.7	3	—	7	—	1.0	36		
	1.832	0.245	1.01	± 0.08	1.75	± 0.17	—	—	—	—	—	1.7	± 0.3	13	± 6	1.9	3	—	7	—	1.2	39		
1984 day 249	0.584	0.144	0.92	± 0.13	0.79	± 0.11	3.1	± 0.2	-1.2	± 0.3	1.6	± 0.3	4.5	± 0.4	147	± 580	1.2	3	—	31.3	—	1.2	34	
	0.810	0.054	0.62	± 0.07	1.35	± 0.20	3.1	± 0.2	-0.7	± 0.2	2.7	± 0.6	4.2	± 0.4	326	$\pm \infty$	1.1	3	—	34.2	—	1.0	34	
1984 day 250	1.090	0.072	0.42	± 0.09	1.3	± 0.3	1.4	—	-0.5	—	2	—	3.7	± 0.3	38	± 12	0.7	3	—	7	—	1.1	37	
	1.253	0.036	0.72	± 0.09	0.93	± 0.12	0.7	—	-0.5	—	2	—	3.1	± 0.3	48	± 39	1.0	3	—	7	—	0.8	37	
1985 day 232	1.440	0.063	1.16	± 0.11	2.17	± 0.21	—	—	—	—	—	—	2.9	± 0.2	31	± 9	1.1	3	—	7	—	1.4	40	
	1.612	0.027	1.13	± 0.05	1.51	± 0.09	—	—	—	—	—	—	2.1	± 0.3	56	± 35	1.2	± 0.2	3.0	± 1.6	7.8	± 0.5	0.8	57
	1.693	0.018	1.46	± 0.07	1.65	± 0.09	—	—	—	—	—	—	2.9	± 0.2	321	$\pm \infty$	1.7	± 0.3	5.2	± 2.4	6.9	± 0.5	1.1	57
	1.756	0.018	1.31	± 0.07	1.62	± 0.11	—	—	—	—	—	—	3.2	± 0.2	112	± 82	1.9	± 0.2	4.4	± 1.2	8.1	± 0.3	1.0	57
	1.810	0.018	2.25	± 0.12	1.71	± 0.08	—	—	—	—	—	—	3.1	± 0.2	269	$\pm \infty$	2.1	± 0.1	3.2	± 0.5	7.2	± 0.2	1.5	57
	1.883	0.036	1.22	± 0.06	1.33	± 0.12	—	—	—	—	—	—	2.4	± 0.6	108	$\pm \infty$	2.7	± 0.5	7.3	± 4.4	6.8	± 0.5	1.1	75
	0.116	0.036	0.47	± 0.04	2.2	± 0.5	3.2	± 0.1	-0.8	± 0.1	1.3	± 0.2	5.4	± 0.3	20	± 1	1.9	± 0.1	2.7	± 0.8	25.7	± 0.3	1.0	105
		0.251	0.072	0.58	± 0.06	1.59	± 0.23	3.6	± 0.1	-0.6	± 0.1	1.7	± 0.1	5.6	± 0.2	34	± 1	1.6	± 0.2	2.8	± 0.5	26.9	± 0.9	0.8
HER7 ^{d,e}	0.007	0.090	0.53	± 0.08	1.5	—	1.6	± 0.3	-1.2	± 0.2	0.7	± 0.6	3.5	± 0.5	18	± 12	1.3	3	—	24.1	—	0.7	28	
	0.296	0.090	0.53	± 0.09	1.42	± 0.20	1.0	± 0.2	-3.1	± 1.6	0.3	± 0.3	3.1	± 1.8	30	± 41	1.7	3	—	27.7	—	0.8	36	
1986 day 093 ^g	1.558	0.099	6.9	± 0.5	2.26	± 0.06	—	—	—	—	—	—	3.1	± 0.2	108	± 66	1.2	3	—	7	—	1.4	40	
	1.801	0.072	6.6	± 0.3	2.09	± 0.04	—	—	—	—	—	—	3.2	± 0.2	41	± 9	1.3	3	—	7	—	1.0	40	
	2.650	0.298	5.6	± 0.3	2.07	± 0.05	—	—	—	—	—	—	3.0	± 0.2	40	± 12	1.2	7	—	16	—	1.0	40	
	3.868	0.406	6.6	± 0.4	1.86	± 0.05	—	—	—	—	—	—	2.4	± 0.3	127	$\pm \infty$	1.1	7	—	16	—	1.3	40	
HTR4 ^{d,f}	2.812	0.162	6.2	± 0.5	1.99	± 0.07	—	—	—	—	—	—	1.7	—	77	—	1.8	7	—	16	—	0.9	41	

^a Whenever a component was not evaluated it is indicated by “—”; whenever we determined an upper limit (1σ) of a component, we indicate the errors of the fixed parameters by “—”. VLFN, LFN and HFN are determined from 0.001–1 Hz, 0.01–100 Hz and 0.01–1000 Hz, respectively.

^b HBO or NBO.

^c All errors are determined from an error scan through the χ^2 space using $\Delta\chi^2 = 1$.

^d The Poisson level was a free parameter in the fits to these data.

^e Effective energy range: 1.4–4.1 keV.

^f Effective energy range: 1.2–19.8 keV.

^g Pointing unstable; VLFN results may be corrupted, see text.

Table 3a: Results of power spectral fits of 16 s FFTs (HB/NB)^a

Obs. period	$\overline{S_Z}$	σ_{S_Z}	VLFN				LFN				HFN				QPO ^b				χ^2_{red}	dof				
			rms	err	α_V	err	rms	err ^c	α_L	err	ν_L (Hz)	err	rms	err	ν_H (Hz)	err	rms	err	$\Delta\nu$ (Hz)	ν (Hz)	err			
1983 day 215	1.351	0.087	0.5	—	1.5	—	1.8	± 0.2	-0.2	± 0.3	2.5	± 1.3	1.4	—	77	—	0.9	3	—	7	—	0.9	37	
	1.832	0.245	0.7	—	1.5	—	—	—	—	—	—	—	1.0	—	77	—	1.8	± 0.3	3.3	± 1.6	6.0	± 0.6	0.8	37
1984 day 249	0.495	0.144	1.2	—	1.5	—	3.7	± 0.2	-0.8	± 0.3	1.9	± 0.5	4.6	± 0.5	99	$\pm \infty$	1.2	3	—	30.2	—	1.4	27	
	0.729	0.027	0.8	—	1.5	—	3.1	± 0.2	-0.8	± 0.2	2.4	± 0.5	4.6	± 0.4	133	$\pm \infty$	1.3	3	—	33.2	—	0.7	27	
	0.838	0.045	0.3	—	1.5	—	2.5	± 0.4	-0.8	± 0.4	2.0	± 1.0	4.1	± 0.4	77	$\pm \infty$	1.0	3	—	34.5	—	1.1	27	
1984 day 250	1.036	0.054	0.7	—	1.5	—	1.6	—	-0.5	—	2	—	3.6	± 0.4	39	± 35	0.4	3	—	7	—	1.4	34	
	1.153	0.027	0.8	—	1.5	—	1.4	—	-0.5	—	2	—	4.0	± 0.4	43	± 15	0.5	3	—	7	—	0.5	34	
	1.226	0.018	0.6	—	1.5	—	0.6	—	-0.5	—	2	—	3.4	± 0.4	68	± 170	0.8	3	—	7	—	1.0	34	
1985 day 258	1.280	0.027	1.0	—	1.5	—	0.9	—	-0.5	—	2	—	2.6	± 0.4	19	± 6	1.2	3	—	7	—	0.6	33	
	0.097	0.036	1.0	—	1.5	—	2.5	± 0.3	-1.7	± 0.6	0.7	± 0.2	5.0	± 0.2	10	± 1	2.7	± 0.3	5.6	± 1.3	25.1	± 0.4	1.3	44
	0.170	0.009	0.7	—	1.5	—	3.8	± 0.2	-0.3	± 0.1	2.2	± 0.3	5.8	± 0.2	32	± 3	1.5	± 0.2	2.0	± 1.0	26.3	± 0.4	1.0	88
HTR4 ^{d,e}	0.287	0.063	0.9	—	1.5	—	3.5	± 0.1	-0.6	± 0.1	1.8	± 0.3	5.8	± 0.2	38	± 4	1.4	± 0.3	1.7	± 0.9	27.3	± 0.6	0.9	72
	0.079	0.090	0.4	—	1.5	—	4.8	± 0.1	-0.1	± 0.1	3.7	± 0.6	6.7	—	77	—	3.4	± 0.3	6.7	± 2.1	24.0	± 0.5	1.2	42
	-0.020 ^g	0.072	1.4	—	1.5	—	1.4	± 0.3	-0.9	± 1.1	0.5	± 0.9	3.7	± 0.5	14	± 5	1.7	3	—	23.8	—	1.1	30	
HER7 ^{d,f}	0.161	0.063	1.0	—	1.5	—	1.4	± 0.2	-5	± 3	0.2	± 0.1	3.1	± 0.5	13	± 2	2.0	3	—	26.1	—	1.0	29	
	0.359	0.054	0.9	—	1.5	—	1.8	—	-0.5	—	2	—	3.6	± 1.6	23	± 35	1.6	3	—	28.5	—	0.8	33	

^aWhenever a component was not evaluated it is indicated by “-”; whenever we determined an upper limit (1 σ) of a component, we indicate the errors of the fixed parameters by “—”. VLFN, LFN and HFN are determined from 0.01–1 Hz, 0.01–100 Hz and 0.01–1000 Hz, respectively.

^bHBO or NBO.

^cAll errors are determined from an error scan through the χ^2 space using $\Delta\chi^2 = 1$.

^dThe Poisson level was a free parameter in the fits to these data.

^eEffective energy range: 1.4–11.5 keV.

^fEffective energy range: 1.4–4.1 keV.

^gNegative S_Z due to scaling; this indicates that the HB is somewhat longer than the NB.

Table 3b: Results of power spectral fits of 16 s FFTs (NB/FB)^a

Obs. period	$\overline{S_Z}$	σ_{S_Z}	VLFN				HFN				QPO ^b				χ^2_{red}	dof		
			rms	err ^c	α_V	err	rms	err	ν_H (Hz)	err	rms	err	$\Delta\nu$ (Hz)	err	ν (Hz)	err		
1985 day 232	1.386	0.027	0.7		1.5	—	3.3	± 0.2	94	± 36	1.3	3	—	7	—	1.3	30	
	1.486	0.045	0.7		1.5	—	2.9	± 0.3	108	± 43	1.5	± 0.3	3.9	± 2.0	5.3	± 0.7	1.0	53
	1.603	0.027	1.0	$+\infty$ -0.3	2.1	$+\infty$ -1.0	2.4	± 0.3	63	$+\infty$ -36	1.3	3	—	7	—	0.8	28	
	1.666	0.009	1.0	$+2.8$ -0.2	1.8	$+2.2$ -0.7	2.8	± 0.3	82	± 42	1.2	3	—	7	—	1.1	28	
	1.711	0.009	0.6		1.5	—	2.9	± 0.5	70	$+94$ -31	1.9	± 0.8	6	± 6	6.8	± 0.9	1.0	53
	1.756	0.009	0.9	± 0.1	1.0	± 0.2	2.9	± 0.3	160	$+116$ -49	1.8	± 0.2	3.4	± 1.2	8.1	± 0.4	1.5	51
	1.801	0.009	0.8	± 0.1	0.9	± 0.3	3.3	± 0.3	141	$+73$ -36	1.9	± 0.2	2.3	± 0.7	7.6	± 0.2	0.8	51
	1.847	0.009	0.9		1.5	—	3.7	± 0.4	33	$+29$ -12	1.9	3	—	7	—	1.8	30	
	1.901	0.027	1.0	± 0.1	1.0	± 0.3	2.8	± 0.3	62	$+77$ -28	2.5	± 0.4	4.1	± 1.6	7.4	± 0.3	0.9	51
	1.495	0.090	1.0	± 0.2	1.6	± 0.5	3.0	± 0.2	82	± 21	1.2	3	—	7	—	1.0	31	
1986 day 093	1.639	0.027	0.8	$+2.7$ -0.1	1.5	$+2.5$ -0.5	3.1	± 0.2	109	± 29	1.0	3	—	7	—	1.2	31	
	1.738	0.027	0.8	± 0.1	1.0	± 0.2	3.2	± 0.2	149	± 34	0.9	3	—	7	—	1.4	31	
	1.856	0.045	0.9	± 0.1	1.3	± 0.5	3.4	± 0.3	105	± 33	1.5	± 0.3	2.7	± 1.1	6.9	± 0.3	0.8	57
	2.361	0.072	1.1	$+0.8$ -0.2	1.6	± 0.7	3.2	± 0.5	131	± 54	2.3	± 0.3	7	± 3	16.1	± 0.6	1.0	57
	2.632	0.108	1.0	± 0.1	1.4	± 0.3	3.1	± 0.3	62	± 19	1.3	7	—	16	—	0.8	31	
	2.993	0.099	2.6	$+1.8$ -0.6	2.5	± 0.6	3.5	± 0.3	52	± 18	1.2	7	—	16	—	1.0	31	
	3.444	0.180	2.4	± 0.2	1.8	± 0.2	2.4	± 0.4	151	$+165$ -74	1.1	7	—	16	—	0.9	31	
	4.157	0.280	3.1	± 0.2	1.9	± 0.2	2.4	± 0.3	132	± 64	0.5	7	—	16	—	0.8	31	
	2.659	0.126	2.1	$+2.6$ -0.5	2.2	$+1.6$ -0.6	2.5	± 0.5	12	± 6	1.0	7	—	16	—	1.2	24	
	3.002	0.126	2.7	$+1.1$ -0.5	2.3	± 0.4	1.3	± 0.7	19	$+\infty$ -11	1.8	7	—	16	—	1.3	24	
	3.823	0.316	3.5	± 0.3	2.0	± 0.2	2.1		77	—	0.9	7	—	16	—	1.5	26	

^aWhenever a component was not evaluated it is indicated by “—”; whenever we determined an upper limit (1σ) of a component, we indicate the errors of the fixed parameters by “—”. VLFN and HFN are determined from 0.01–1 Hz and 0.01–100 Hz, respectively.

^bNBO or FBO.

^cAll errors are determined from an error scan through the χ^2 space using $\Delta\chi^2 = 1$.

^dThe Poisson level was a free parameter in the fits to these data. Effective energy range: 1.2–19.8 keV.

Table 5: Upper limits to modulation strength

Burst	ν_{Ny}^a (Hz)	Upper limit (%) ^b
I	64	6.1
II	256	1.0
III	512	2.1
IV	512	1.9
II+III+IV	256	0.9
III+IV	512	1.5

^a ν_{Ny} is the Nyquist frequency.^b99 per cent confidence upper limit to the fractional sinusoidal amplitude of the total flux.**Table 6:** Polar cap areas (km^2)^a

r_m^b (km)	Dipole field offset (km)					
	0	1	2	3	4	5
15	259	325	389	456	519	591
	259	214	157	109	70	41
40	84	110	140	172	207	245
	84	68	49	33	22	13
100	33	43	55	69	86	106
	33	26	19	13	8	5

^aTotal area of the neutron star is $\sim 1257 \text{ km}^2$.^b r_m is the magnetospheric radius.**Table A1:** EXOSAT Argon HER7 observation log

Source	Year	Date	Day ^a	Time Resolution	Spectral State
GX 5-1	1985	Aug 27/28	239/240	3.9 ms	NB/FB
	1985	Aug 29	241	3.9 ms	NB
	1985	Aug 30	242	3.9 ms	NB
	1985	Sep 17	260	3.9 ms	HB
Cyg X-2	1985	Oct 28/29	301/302	3.9 ms	HB
	1985	Oct 29	302	3.9 ms	HB
	1985	Nov 14/15	318/319	3.9 ms	NB/FB
GX 17+2	1986	Apr 3/4	093/094	7.8 ms	NB/FB
Sco X-1	1985	Aug 24	236	3.9 ms	FB
	1985	Aug 25	237	3.9 ms	NB/FB
	1986	Mar 11/12	070/071	7.8 ms	HB/NB
	1986	Mar 13/14	072/073	3.9/7.8 ms	NB
GX 3+1	1985	Sep 4	247	3.9 ms	UB ^b

^aJan 1 = day 1.^bUB = upper banana (see Hasinger & van der Klis 1989).